EarthArXiv preprint – this manuscript is not peer reviewed

Foraminiferal Analysis of Holocene Sea Level Rise within the Trinity River Incised Paleo-Valley, Offshore Galveston Bay, Texas

Standring, P.[1,2]*, Lowery, C.M. [1], Burstein, J. [1,2,^], Swartz, J. [1,2,#], Goff, J. A. [1], Gulick, S.P.S. [1,2], Miller, C.B.[1,2]

[1]Institute for Geophysics, University of Texas at Austin, Austin, Texas

[2]Department of Earth and Planetary Sciences, University of Texas at Austin, Austin, Texas

*Corresponding Author: patty.standring@utexas.edu

[#]Now at: Water Institute of the Gulf, Baton Rouge, Louisiana

[^]Now at: OARS Group – Marine Geoscience Consultants, Houston, Texas

This manuscript is a non-peer reviewed EarthArXiv preprint. It is currently being reviewed by Marine Geology.

EarthArXiv preprint – this manuscript is not peer reviewed

Highlights:

- Micropaleontology as environmental context for seismic and sedimentological analysis
- Long-term (~2 kyr) stable estuary amid early Holocene sea level rise
- Early Holocene paleoestuary changes dominated by rate of sea level rise
- Middle Holocene transgression influenced by regional climate

Abstract

Regional variability of global sea level rise remains an important area of study given the vulnerability of sediment-starved coastlines to coastal inundation, especially those in proximity to large population centers. Galveston Bay, Texas, is currently experiencing more than double the global rate of sea level rise and is particularly vulnerable to storm inundation that will further destabilize the coastline. Limitations in instrumental observations necessitate the use of the geologic record preserved offshore modern Galveston Bay to understand how this particular coastline responds to periods of rapid sea level rise. We present micropaleontological analysis of sediment cores combined with high-resolution seismic data to reconstruct the Holocene paleoestuary offshore Galveston Bay and its evolution since initial inundation ~10 ka through marine transgression ~6 ka. We find that despite rapid sea level rise, the Galveston paleoestuary maintained relatively stable outer boundaries, and within the bay environmental shifts occurred as a result of probable marine incursions due to tidal inlet migrations. Paleoenvironmental changes in the early Holocene coincide with flooding events within other Texas Gulf Coast bays suggesting global sea level rise played a prominent role. Middle to late Holocene changes occurred when rates of sea level rise slowed, suggesting regional hydroclimate change played a more dominant role.

EarthArXiv preprint – this manuscript is not peer reviewed

Keywords: Sea level change, micropaleontology (forams), N America

1. Introduction

Constraining the regionally variable impact of rising sea level is increasingly important for coastal planning (Vitousek et al., 2017). Regional variability of sea level rise is particularly evident in Galveston Bay, Texas. Low-gradient, low-elevation coastlines all around the Gulf of Mexico are especially vulnerable to sea level rise and the destruction caused by large storms and hurricanes (Bernstein et al., 2019; FitzGerald et al., 2008; Goff et al., 2010; Palermo et al., 2021; Shawler et al., 2021). Mean annual sea level rates at Galveston Bay Pier 21 are +6.63 ± 0.21 mm yr^{-1} from 1904-2020 (NOAA, 2023). This rate is significantly higher than all other stations along the Texas Coast, and even double in some cases. For example, South Padre Island and Port Mansfield in south Texas are experiencing rates of sea level rise of +4.23 ± 0.51 mm yr^{-1} and +3.69 ± 0.66 mm yr^{-1}, respectively (NOAA, 2023).

The modern rate of sea level rise in Galveston Bay exceeds that of the last 10 kyr, when waning melting of ice sheets slowed global sea level rise from 4.2 mm yr^{-1} to 1.4 mm yr^{-1} (Anderson et al., 2022; Milliken et al., 2008a). Extensive work by John Anderson and colleagues in several Gulf Coast estuaries revealed several rapid flooding events when the entire estuary and barrier island system retreated landward by several kilometers (Anderson et al., 2022, 2016, 2014, 2008; Anderson and Rodriguez, 2008; Maddox et al., 2008; Milliken et al., 2008a; 2008b; 2008c; Rodriguez, 1999; Rodriguez et al., 2008a, 2008b, 2005, 2004, 2001, 1999; Simms et al., 2008; Siringan, 1993; Siringan and Anderson, 1994; 1993; Thomas and Anderson, 1994). These

major events occurred on the order of ~1000 years, and apparently punctuated intervals of relative stability. An estuary can be considered stable while maintaining its external boundaries (i.e., barrier island system) and still undergo environmental change within the estuary (e.g., salinity variability due to increased marine mixing or higher fluvial input). Characterizing those intervals of stability is essential for understanding how the modern Galveston Bay system will respond to renewed sea level rise. Can change occur during these periods of stability? Is there a sea level threshold that produces estuarine instability in the system? The physics are currently unclear.

Benthic foraminiferal assemblages provide a sensitive indicator of bay environment that can record more gradual changes than those typically reconstructed from mollusks in core samples. Here, we integrate high-resolution seismic data published by Burstein et al. (2023) and Swartz et al. (2022) with micropaleontological analysis, sedimentology, and a radiocarbon-based age model from sediment cores in the paleo-Trinity estuary system offshore of modern Galveston Bay (Figure 1) to develop a comprehensive history of Holocene paleoenvironmental and coastal change in the Trinity paleo-valley over the last 10 kyr. We identify periods in which barrier island development helped maintain a stable paleoestuary prior to marine transgression.

2. Regional Setting/Background

Galveston Bay is located on the northeast Texas coast on the Gulf of Mexico and consists of three bays (East, Trinity, and Galveston bays) that comprise the estuary complex (Figure 1). The microtidal, wave-dominated regime in the Gulf of Mexico allows for long, narrow, relatively straight barrier island system protecting the estuary, consisting of Bolivar Peninsula on the

eastern side of the bay and Galveston Island on the western side (Anderson et al., 2016; 2014; 2008; Davis and Hayes, 1984; FitzGerald et al., 2008; Rodriguez et al., 2004).

John Anderson and colleagues at Rice University established a firm foundation of research on modern Galveston Bay and its transformation throughout the Holocene (Anderson et al., 2022; 2016; 2014; 2008; Milliken et al., 2008a; Rodriguez et al., 2005; 2004; Simms et al., 2007; Siringan and Anderson, 1993; Thomas and Anderson, 1994). During Marine Isotope Stages (MIS) 5-3, the region experienced episodic sea level fall, which led to the creation of Trinity and San Jacinto incised river valley (Figure 2A & 2C) (Anderson et al., 2016; 2014; Swartz et al., 2022). Stepped downcutting throughout the incised valley resulted in terraced morphology (Anderson et al., 2016; 2008; Rodriguez et al., 2005). The upper, wider portions of the offshore incised valley are not visible in the sediment record because this stratigraphy has been removed by shoreface erosion due to the transgressive ravinement during Holocene sea level rise. This ravinement occurs at 8 to 10 m depth below the seafloor along the Texas coast, expressed as onlapping marine muds onto a “decapitated shoreface” (Anderson et al., 2016).

Global sea level rise between ~11.4 and 8.2 ka is estimated at ~15 m kyr^{-1} followed by a reduced rate of sea level rise 8.2-6.7 ka, coinciding with the final deglaciation of North America (Lambeck et al., 2014). Along the Gulf Coast, sea level began to rise episodically between ~10 and 7 ka, after which it slowed to steady present day levels (Figure 2B) (Anderson et al., 2016; 2014; Milliken et al., 2008a; Swartz, 2019). Multiple proposed flooding surfaces within the Trinity incised valley occur either contemporaneously with other areas along the Gulf coast and are attributed to rapid sea level rise, or exist locally, suggesting forcing mechanisms such as changing sediment supply and/or antecedent topography (Anderson et al, 2022, 2016;

Rodriguez et al., 2005). Radiocarbon dating in sediment cores from modern Galveston Bay constrain rapid sea level rise events to 9.6 ka, 8.2 ka, and between 7.7 and 7.4 ka, in which each inundation was complete after only a few centuries (Figure 2B & 3) (Anderson et al., 2022, 2008). Milliken et al. (2008a) identified flooding events consistent with radiocarbon dates and relative sea level changes within the Gulf of Mexico at 9.5-9.8 ka, 8.5-8.9 ka, 8.0-8.4 ka, and 6.8-7.4 ka (Figure 2B).

Approximately 9.6 ka, the initial inundation of modern Galveston Bay shifted the upper bay ~30 km up the incised valley, coincident with Laurentide Ice Sheet (LIS) retreat and Hudson Strait freshwater drainage (Anderson et al., 2008; Jennings et al., 2015; Lambeck et al., 2014; Thomas and Anderson, 1994) and is primarily attributed to antecedent topography coinciding with rapid sea level rise events (Anderson et al., 2022; Rodriguez et al., 2008b, 2005). Approximately 8.2 ka, the bayhead delta shifted ~10 km up the valley, partially attributed to a "dramatic decrease in sedimentation rates" from 4.6 mm yr^{-1} to 1.3 mm yr^{-1} and the elevation of a Pleistocene-age terrace (Figure 3, Anderson et al., 2008) but coinciding with LIS melting events at ~8.6 ka and 8.15 ka (Jennings et al., 2015). Between 7.7 and 7.4 ka the upper bay shifted a farther ~25 km up the valley at a rate of 8 km $century^{-1}$ but maintained its existing shoreline ~50 km seaward of the modern coastline, which produced a ~100-km-long paleoestuary (Anderson et al., 2008; Rodriguez et al., 2005). This flooding event occurred despite the decreasing rate of sea level rise between 7.5 and 7.0 ka, with coincident events in Matagorda Bay (Maddox et al., 2008) and Sabine Lake (Milliken et al., 2008c), and is attributed to a Gulf Coast climate transition from cool and moist to warm and dry regimes, reducing sediment supply (Anderson et al., 2008).

EarthArXiv preprint – this manuscript is not peer reviewed

Radiocarbon dating of sediments from Heald Bank suggest that the paleoshoreline was in that location by as late as 7.7 ka, while ages obtained from the oldest beach ridges on Galveston Island constrain the seaward progradation of the island to after 5.3 ka (Figure 2A) (Anderson et al., 2014; 2008; Rodriguez et al., 2005; 2004). Prior interpretations of Heald Bank suggest the bank may be marine in origin, like Thomas and Shepard Banks, and developed after the shoreline had already shifted up-valley (Thomas and Anderson, 1994). Bolivar Peninsula began to develop as a spit ~2.5 ka and as it prograded westward, the tidal inlet narrowed to a fraction of its original size to form Bolivar Roads tidal inlet allowing flooding along the bay boundaries, establishing the modern shape of Galveston Bay (Anderson et al., 2016; 2014; 2008; Rodriguez et al., 2005; 2004).

Although prior sedimentological, radiocarbon, and seismic research offshore Galveston Bay is thorough (Anderson et al., 2022; 2016; 2008; Rodriguez, 1999; Rodriguez et al., 2004), additional higher resolution seismic data combined with radiocarbon dating of sediment cores and micropaleontological interpretations of facies changes will better spatially and temporally constrain the large estuarine environment and the transformation of the coastline throughout the Holocene. Foraminifera are powerful proxies for paleoenvironmental and relative sea level change because of their sensitivity to temperature, salinity, and nutrient availability (Culver, 1988; Culver et al., 1996; Garrett et al., 2023; Gehrels, 2013; Leckie and Olson, 2003; Phleger, 1951; Poag, 2015, 1981; Williams, 1994; Woo et al., 1997). Modern assemblages represent a specific physical and chemical environment within ecological niches or biozones that can be translated to fossil assemblages in sediment cores to identify paleoenvironmental changes as a result of relative sea level fluctuations forming a link between observational and fossil records

EarthArXiv preprint – this manuscript is not peer reviewed

(Culver, 1988; Gehrels, 2013; Leckie and Olson, 2003; Phleger, 1965; 1960; Poag, 1981). Foraminiferal paleoecological assemblages have been used extensively to reconstruct depositional environmental change (e.g., Buzas-Stephens et al., 2014; Olson and Leckie, 2003; Wellner et al., 2004). Extensive work on the living assemblages of Galveston Bay was carried out by Wantland (1969) and was combined with unpublished data from William Sliter by Poag (1981) to provide detailed maps of foraminiferal predominance facies in the bay. This assemblage work allows us to differentiate upper, middle, and outer (sometimes referred to as lower) bay environments within otherwise unremarkable successions of estuarine mud and separate sandy ebb- and flood-tidal delta deposits from back-barrier, washover fans. Benthic foraminiferal assemblages provide paleoenvironmental context for seismic data and allow for the clarification of the timing of the inundation of the Trinity River Paleo-valley and the interpretation of barrier island stability and rollover rate amid rising sea levels at a higher resolution than has previously been possible.

3. Methods

3.1 *Seismic Data*

Approximately 700 km of high-resolution seismic data were collected during three cruises in 2017 to 2018. These surveys were conducted with an EdgeTech 512i sub-bottom profiler with 0.7 to 12 kHz frequency sweep and 20-ms pulse length (Figure 1). Extensive discussion of seismic data processing and interpretation (including images of uninterpreted lines) can be found in Swartz et al. (2022) and Burstein et al. (2023). Seismic lines corresponding to sediment cores were converted from two-way travel time in milliseconds to meters with an

EarthArXiv preprint – this manuscript is not peer reviewed

177 approximate seismic wave velocity of 1525 m s^{-1} based on average values from Exxon surveys of
178 the Brazos River delta region to the west of our study area (Abdulah et al., 2004).
179
180 3.2 *Piston and gravity coring*
181 Piston core (PC) sites (Figure 1) were chosen based on sedimentary structures observed
182 in seismic data to pinpoint key transitions in the sedimentary record and evaluate
183 paleoenvironmental evolution from fluvial to estuarine to modern-day marine. The cores were
184 collected on the R/V *Brooks McCall* during the University of Texas Institute for Geophysics 2018
185 Marine Geology and Geophysics (MG&G) Field Course. Gravity cores (GC) were collected on a
186 subsequent cruise of the R/V *Manta* in 2019 (Figure 1) and were located to clarify additional
187 seismic horizons of interest, particularly along the valley edges.
188 Cores were split onshore after both cruises were completed. The archive halves were
189 stored, and the working halves were described for appearance, qualitative grain size,
190 bioturbation, and presence of marine fauna (e.g., shell fragments and shell hash), and terrestrial
191 organic material (e.g., plant debris) and then sampled for quantitative grain size analysis,
192 microfossil analysis, and carbon dating. Microfossil analysis samples (~10 cm^3 of material) were
193 selected at 10- to 50-cm intervals, and at specific points where a paleoenvironmental transition
194 may have occurred based on changes observed in the core, generally avoiding sandier
195 sediments, which tend to contain few (and often reworked) foraminifera. Piston core 2 (PC-2)
196 was the longest core collected and was sampled at higher resolution to serve as a reference
197 section. Subsequent sampling in PC-4 and all the gravity cores (GC-1 through GC-6) was done at
198 a lower resolution with additional samples selected to more precisely identify

EarthArXiv preprint – this manuscript is not peer reviewed

paleoenvironmental transitions. Samples were soaked for at least 24 hours in a mixture of borax and hydrogen peroxide to break down clay floccules, washed over a 63-µm sieve, and dried in an oven at low temperatures (~75°C).

3.3 *Foraminiferal analysis*

Population abundance analysis is more robust than presence/absence of fossil material in identifying depositional environmental change, and more sensitive to subtle changes. Samples were split in a microsplitter to provide a reasonable amount of material and foraminifera were picked using a binocular microscope in a randomized pattern to avoid bias and placed on a slide. Population sizes of at least 100 foraminifera tests were picked where possible (some samples were barren or did not yield 100 individuals) and identified at the genus level. Foraminifera that were not identifiable at the genus level were classified as "benthic spp." Confidence interval calculations (Appendix A) following the binomial method of Buzas (1990) show that these population sizes are sufficient to track changes in predominance facies (i.e., *Ammonia* vs. *Elphidium*) within the estuary and recent analysis shows that populations of at least 58 individuals in low diversity assemblages are sufficient for statistical purposes (Forcino et al., 2015). Several modern grab samples from Bolivar Roads tidal inlet obtained during the MG&G 2018 Field Course were analyzed and used as a comparison for flood- and ebb-tidal delta sediments in the cores. Grab samples were soaked overnight in a 1% solution of Rose Bengal and water immediately after collection to stain specimens which were living or recently living. Samples were then sieved and dried in an oven at low temperatures (~75°C). Populations (living

EarthArXiv preprint – this manuscript is not peer reviewed

and total) of at least 300 individuals were picked and identified at the genus level (see Appendix A).

Foraminiferal predominance facies in the Gulf of Mexico are defined by genus (Culver, 1988; Poag, 1981). Poag (1981) synthesized analysis of modern benthic foraminiferal assemblages in the Gulf (Figure 4) and outlined predominance facies for Galveston estuary complex based on the previous work conducted by Wantland (1969) within the Trinity Bay and unpublished work from William V. Sliter of the USGS. Wantland (1969) collected 87 samples from stations within the subaerial Trinity River delta and Trinity Bay and used Rose Bengal solution to determine live taxa at time of collection. Live samples were picked from 62-µm sieved wet sediments and populations were based on at least 300 individual tests where possible (Wantland, 1969). Poag (1981) identified the following modern predominance facies for Galveston Bay: dominance of *Ammotium* indicates upper bay or river delta facies (sometimes referred to as bayhead delta), dominance of *Ammonia* indicates central bay facies, and dominance of *Elphidium* indicates outer bay (sometimes referred to as lower bay) facies (Figure 4). In an effort to match Poag (1981)'s predominance facies, we adopt the terminology of upper bay when describing portions of the estuary that are proximal to the river delta are fresher and outer bay for more saline areas closer to the estuary mouth. Culver (1988) also outlined a priori groups of prominent foraminifera genera by depth and environmental preference, which match well with Poag's predominance facies. Culver (1988)'s diagnostic genera include, *Ammotium* for marshes, *Ammobaculites* and *Elphidium* for bays/estuaries, and *Bolivina*, *Bulimina*, and *Elphidium* for inner shelf environments (Figure 4).

EarthArXiv preprint – this manuscript is not peer reviewed

Paleoenvironmental interpretations of the Holocene estuary system are based off of assemblage percentages of three primary genera outlined by Poag (1981). Samples with >50% *Ammonia* are interpreted as central bay facies, samples with ~50-50 *Ammonia/Elphidium* are transitional to outer bay, and samples with >50% *Elphidium* are outer bay facies. *Ammotium*, indicative of Poag's upper bay (bayhead delta) facies, was very rare and poorly preserved in our cores, as were agglutinated taxa more generally, and so we lumped them all together as agglutinated spp. An overall increase in diversity including common inner shelf taxa (e.g., *Bulimina, Bolivina*, miliolids, etc.), typically coupled with a resurgence of *Ammonia* spp., likely indicates a transition to modern marine or open shelf facies (Culver, 1988; Leckie and Olson, 2003; Poag, 1981).

Estuaries are dynamic environments and reworking of material is likely common. To identify areas of potential reworking, foraminiferal test fragments (interpreted to be broken during redeposition) within each sample were counted in addition to individual identifiable tests for population totals. Total fragments were normalized to total foraminifera to provide a percent fragmentation for each sample. Peaks in fragmentation are interpreted as potential periods of increased energy or sediment reworking.

3.4 *Radiocarbon dating*

Sediment cores were sampled for radiocarbon dating to provide age constraints on paleoenvironmental transitions and develop age models for each core. A total of 28 samples were sent to the National Ocean Sciences Accelerator Mass Spectrometry (NOSAMS) at Woods Hole Oceanographic Institute for radiocarbon dating using the Libby half-life of 5,568 yr and

corrected for carbon isotopic fractionation. Of these samples, 23 were mollusk shells, 2 were comprised of foraminiferal tests, and 3 were plant debris (Table 1). Attempts were made to select articulated mollusk shells for dating, but the absence of these shells precluded their use for radiocarbon dating. Mollusk shell species were not identified because it was deemed unnecessary to use macrofauna as depositional environmental indicators in conjunction with the more precise foraminiferal population analysis.

At NOSAMS, mollusk and foraminiferal samples containing at least 4 mg of material underwent hydrolysis where carbon in the samples were converted to CO_2 using a strong acid H_2PO_3. Mollusk samples were powdered to allow staff to subsample material >9 mg. Radiocarbon dates from plant material were calibrated with IntCal20 (Reimer et al., 2020) and mollusk and foraminifera ages were corrected for reservoir variations using a correction specific to the Gulf of Mexico offshore Galveston Bay (Wagner et al., 2009) and then calibrated using Marine20 (Heaton et al., 2020). The IntCal20 calibrations were done via the online program OxCal 4.4 (Ramsey, 2009) and the Marine20 calibrations were applied through the R package Bchron (Haslett and Parnell, 2008). Errors in ages were calculated by NOSAMS where the error is determined by the larger of two estimates, the internal statistical error calculated using the total number of ^{14}C counts (error = $1/\sqrt{n}$) and the external error determined by the ratio of ^{14}C and ^{12}C of a sample calculated 10 separate times while the sample was being run.

3.5 *Age models*

Age models were developed using the R code rbacon (Blaauw and Christen, 2011), which calculates sediment accumulation rates based on a gamma autoregressive semiparametric

EarthArXiv preprint – this manuscript is not peer reviewed

model using a Markhov chain Monte Carlo algorithm. The model provides a predictive window with 95% confidence of the age of sediments given depth and radiocarbon age constraints and the assumption of consistent deposition unless hiatuses are applied. Although we suspect a significant amount of erosion may have occurred during transgression, the lack of upper core (modern marine inner shelf) carbon dates limits the application of hiatus depths in the model and extrapolated ages for the upper core are likely incorrect. Interpolated ages from the models for each core (except for GC-1) were used to date environmental transitions between radiocarbon ages, and in a few instances, extrapolated ages were used to identify transitions outside the range of carbon dates.

3.6 *Grain size analysis*

Sediment samples were taken from PC-2, PC-4, GC-5, and GC-6 at 5-30 cm intervals that varied by core depending on qualitative sedimentology. Samples were dried and then soaked in deionized water for 24 hrs prior to analysis. Samples were then ultrasonified and stirred before transfer to the Malvern Mastersizer 3000 laser grain size analyzer via pipette until obscuration levels reached the required optimum level for analysis. Quantitative grain sizes between 1 and 1000 µm were then used to determine percent abundance of clay, silt, and sand size fractions.

4. Results

Sediment cores range from <1 m to ~6.3 m in depth and primarily contain medium-gray mud predominantly composed of clayey-silt with sandy intervals that occasionally coincide with shell hash layers or abundant shell fragments. GC-4 contains more organic material and less

EarthArXiv preprint – this manuscript is not peer reviewed

shell material than all the other cores. GC-1 and PC-4 contain sharp and gradual contacts, respectively, between stiff, light-gray Pleistocene clay terraces and Holocene sediments. PC-2 and PC-4 did not contain any analyzable upper seafloor sediments due to coring disturbance. In both cores, the upper core section (0-1 m in PC-4 and 0-1.8 m in PC-2) contains watery mud which sloshed around inside the core liner as the core was brought on deck and laid down to be extruded. These uppermost sections were not split and are included on the stratigraphic columns for these cores as fine mud, with symbols to indicate coring disturbance. Here, we summarize the key observations for each core, proceeding from the most proximal to most distal core.

4.1 *Piston core (PC) 2*

PC-2 was selected for identification of a fluvial terrace toward the western edge of the incised valley (Figure 5A). It consists primarily of massive medium-gray clayey-silt with sporadic sandy intervals of varying thickness (2-10 cm) that coincide with increased shell fragments and in some cases shell hash layers (Figure 5). The core catcher contains silty medium sand (Figure 5). As the reference section representing the complete transition from fluvial to outer bay deposition, this core was sampled at the highest resolution at least every 10 cm (black stars, Figure 5B) and, thus, contains more variability in foraminiferal abundance analysis due to salinity variability within the paleoestuary through time. Foram-based facies changes in PC-2 do not exactly line up with seismic horizons interpreted by Burstein et al. (2023) (Figure 5), possibly due to the higher sensitivity of foraminifera to environmental change than is visible in geophysical data.

EarthArXiv preprint – this manuscript is not peer reviewed

PC-2 is barren of foraminifera from 6.25 to 5.9 m, and we interpret these sandy deposits as fluvial. Barren sediments are overlain by an interval dominated by agglutinated foraminifera (5.9-5.5 m). A mollusk shell at 5.75 m has an age of 9,794 ± 215 cal yr B.P. (Figure 5). By interpolating the sedimentation rate above this sample, we date the top of this unit to ~9.6 ka. From 5.5 to 2.75 m, the core is characterized by a predominance of *Ammonia*, indicating a central bay environment. It is interesting to note that this interval is not uniformly dominated by *Ammonia*, but rather there are also brief increases in *Elphidium*, which may correspond to shifts in salinity caused by migrating position of the inlet or by centennial-scale changes in Trinity River discharge (see Discussion section). Interpolated ages from the age model of this core (Figure 7B) indicates that this central estuary assemblage existed from at least 9.6 to 8.0 ka, indicating a long period of stability in the estuary system during this time. A mollusk shell at 2.48 m within sediments dominated by *Elphidium* has an age of 7,800 ± 134 cal yr B.P., indicating the environment had transitioned to outer bay by ~8.0-7.8 ka. The uppermost ~1.7 m of the core was not analyzed due to coring disturbance.

4.2 *Piston core 4*

PC-4 and subsequent cores were sampled at a lower resolution (black stars, Figure 6B) than PC-2 (Figure 5B), therefore the foraminiferal assemblage changes within these cores appear more gradual compared to PC-2. PC-4 was obtained at the location of another fluvial terrace originally interpreted seismically to be a point bar based on seismic data (Figure 6), but which was instead revealed to be a Pleistocene flood plain deposit comprised of light-gray, stiff Beaumont Clay, into which the MIS5-MIS3 river valley was incised. The terrace is heavily

laminated with oxidized sand layers from subaerial exposure (Figure 6), diagnostic for Pleistocene sediments along the Gulf Coast (Milliken et al., 2008a), and contains a calcareous nodule, which are relatively common in the Beaumont Clay (Rehkemper, 1969). The terrace gradually transitions upward into heavily burrowed sand at ~4.4 m depth, and both the terrace and the overlying sandy section (3.7-5.5 m depth) are barren of microfossils and interpreted as fluvial/terrestrial sediments (Figure 6). At approximately 3.5 m depth, foraminiferal assemblages appear in the sandy sediments and indicate a transition to an upper bay environment. These sediments contain a mollusk shell at 3.44 m depth with an age of 9,131 ± 158 cal yr B.P. and visible burrows with a higher percentage of fragmented foraminifera tests. An extrapolated age from the age model suggests the transition to upper bay took place at ~9.8 ka. Central bay sediments (~2.0-2.9 m depth) are dominated by *Ammonia* and contained a mollusk shell at 2.66 m depth dated to 8,815 ± 175 cal yr B.P. PC-4 contains less central bay sediments (~0.9 m thick) compared to PC-2 (~2.75 m thick), likely due to the elevation of the Pleistocene terrace. The seismic data show draping of sediments above and over the terrace (Figure 6A). At approximately 2 m depth, *Elphidium* becomes more dominant and the environment transitions to outer bay sediments. According to the age model for this core (Figure 6B), the central bay to outer bay transition occurred ~8.0 ka, coinciding with the same transition in PC-2. While fragmentation of tests appears low throughout the core, there is a slight increase in the number of fragments in the outer bay section of the core (1.1-2.0 m depth), indicating a higher energy environment. The increase in diversity of foraminifera at ~1.30 m depth (e.g., increase in common inner shelf genera, like *Bulimina* and *Bolivina*, and some agglutinated taxa) indicates the beginning of a transition to open marine/inner shelf sediments. This section contains two

EarthArXiv preprint – this manuscript is not peer reviewed

carbon dates at approximately the same depth (1.59 m) from mollusk shells, one of which likely contains reworked material because it records an unreasonable age for sediments filling a Holocene estuary (41,030 ± 1,703 cal yrs B.P.). The other shell has an age of 7,787 ± 136 cal yr B.P. for these outer bay sediments. The upper 1 m section of PC-4 also consisted of soft, disturbed material not suitable for sampling.

4.3 *Gravity core (GC) 6*

Along the eastern edge of the paleovalley, GC-6 penetrated bright seismic reflectors that are represented in the core as a ~0.8 m thick sandy package of sediments atop medium-gray estuarine sediments (Figure 7). Starting at the base of GC-6, clay-sized sediments are dominated by *Ammonia*, indicating a central bay environment; a mollusk shell at ~2.1 m depth indicates an age of 8,367 ± 181 Cal yrs B.P. An increase in *Elphidium* at ~1.7 m depth, with an approximate interpolated age of 8.2 ka based on the age model, indicates a transition to outer bay environment (Figure 7B). Smaller sandy intervals at the top of the outer bay sediments provide mollusk carbon dates of 7,709 ± 147 Cal yr B.P. (~1.3 m depth) and 7,760 ± 142 Cal yr B.P. (~1.1 m depth) preceding an irregular contact with the sandy package of sediments (Figure 7B). Shell fragments decrease in abundance going up the core, while foraminifer test fragmentation increases going up the core, suggesting that the sandy package contains reworked material. A mollusk shell within the sandy package has an age of 4,319 ± 165 Cal yrs B.P. Foraminiferal populations suggest a transition from outer bay to inner shelf (increase in inner shelf taxa) was occurring starting at ~1.1 m depth, with the exception of the uppermost sample (GC-6 7-8.5). This uppermost sample contained a foram assemblage that did not match any other

assemblages in the study area cores, so it was compared to modern foraminifera assemblages obtained by Phleger (1965) from Galveston Lagoon on Galveston Island, Surfs Oak on the western edge of Galveston Bay, the Trinity River delta, and two grab samples taken from within the flood- and ebb-tidal areas of Bolivar Roads tidal inlet by the MGG 2018 Field Course (Figure 8, Appendix A). A similar method of foram assemblage comparison was used by Hawkes and Horton (2012) to identify inner shelf-sourced washover sediments from Hurricane Ike on Galveston and San Luis Islands. Our GC-6 comparison revealed that the uppermost sample most closely resembles Phleger's Station 11 sample from Galveston Lagoon (Figure 8). The lack of extensive plant debris indicates that this is not an in situ back-barrier marsh environment. Rather, we interpret this sandy package as transgressive lag containing reworked barrier island marsh sediments.

4.4 *Gravity cores 4 and 5*

GC-4 and GC-5 are ~1500 m apart and sample two different seismic facies along parallel seismic lines separated by 1000-1200 m. Both cores contain central bay sediments, with GC-4 close to the lateral margin of the bay and GC-5 closer to the middle. (Figure 9 & 10). GC-4 penetrates seismic facies along the margin of the incised valley which may explain why it contains the lowest populations of foraminifera of all the cores (all samples are less than 100 individuals), recording intervals of bay margin sediments barren of foraminifera within central bay and outer bay environments (Figure 9B). GC-4 primarily consists of medium-gray clayey-silt with a relatively higher amount of organic material, lower amount of shell fragments, lower foraminiferal test fragmentation compared to other cores (the peak in fragmentation is likely an

417 artifact of lower foram population), and more visible burrowing (Figure 9B). The base of the
418 core contains a barren section (~2.85-3.65 m depth), which is interpreted as bay margin
419 deposits. Plant fragments obtained from 3.35 m depth within these barren sediments were
420 dated to 8,470 ± 144 Cal yr B.P. These deposits transition to central bay sediments at ~2.2 m
421 depth, where they are dominated by *Ammonia* and *Elphidium*, and contain less organic material
422 and more burrowing and shell fragments (Figure 9B). An interpolated age from the age model
423 for this core indicates the transition took place ~8.3 ka. At 1.2 m depth, sediments are again
424 barren of foraminifera and characterized by burrows. Plant fragments from 0.82 m depth have
425 an age of 7,977 ± 221 Cal yr B.P. and the age model interpolates the transition to bay margin at
426 ~1.4 m depth to ~8.1 ka. The upper section of the core contains a thin sand interval with plant
427 debris at 0.56 m dated to 7,913 ± 255 Cal yrs B.P. and is capped by a section of silty sediments.
428 The foraminiferal assemblage in this section is dominated by *Ammonia* and *Elphidium* with a
429 slight increase in agglutinated and common inner shelf taxa indicating a transition to outer bay
430 (~0.5 m depth) and then inner shelf deposits (~0.15 m depth).

431 GC-5 penetrated central bay sediments capped by outer bay deposits (Figure 10). The
432 base of GC-5 contains medium-gray clayey-silt with shell fragments, and a single burrow (Figure
433 10). Shell material from 2.92 m depth has an age of 8,467 ± 130 cal yr B.P. and foraminifera are
434 dominated by *Ammonia*. An interpolated age from the age model (Figure 10B) indicates the
435 central bay to outer bay transition occurred ~8.4 ka (~2.7 m depth). The outer bay sediments
436 are comprised of medium-gray clayey-silt containing sporadic 2-4 cm-scale sandy layers that
437 thicken toward the top of the core to decimeter scale layers with more shell fragments. From
438 ~0.5-1.4 m depth there is an increase in foram fragmentation and sediments are dominated by

EarthArXiv preprint – this manuscript is not peer reviewed

Elphidium. Increasing diversity of foraminifera and presence of agglutinated forams beginning at 1.0 m depth to the top of the core indicate a gradual transition from outer bay depositional environment to modern day marine inner shelf. The peak in fragmentation at approximately 1.0 m depth coincides with a peak in dominance of *Ammonia* and suggests that the increase in *Ammonia* likely represents reworked material. The outer bay section contains mollusk shell fragments that were dated to 8,445 ± 135 cal yr B.P. at 2.50 m depth and 6,661 ± 169 cal yr B.P. at 0.73 m depth (near the top), indicating potential ages for these sediments.

4.5 *Gravity core 1*

GC-1 is extremely short (0.35 m total length; Figure 11). Its location was selected to investigate dipping reflectors seen in seismic data hypothesized to be a Holocene-aged point bar deposit of a tributary at the edge of the Trinity Paleovalley (Figure 11). Instead, the core penetrated a Pleistocene-age terrace containing sticky, dense, burrowed Beaumont Clay. This clay is capped by burrowed sand and thick shell hash and has a sharp contact with modern inner shelf deposits at approximately 0.14 m depth (Figure 11C). Foraminiferal analysis revealed a large population of foraminifera, dominated by *Elphidium,* within one of the burrows of the terrace (see Appendix A). Carbon dating of these foraminifera tests revealed an age of 38,081 ± 1,833 cal yr B.P. almost certainly owing to the inclusion of older material, potentially in the form of dissolved inorganic carbon from the Beaumont Clay. Samples at the terrace contact (0.14 m depth) contained populations of foraminifera dominated by *Ammonia.* Sediments above the terrace contact were dominated by both *Elphidium* and *Ammonia* with a slight increase in

EarthArXiv preprint – this manuscript is not peer reviewed

agglutinated forams and a prominent increase in inner shelf genera, indicating a modern marine environment.

To test radiocarbon dating of different calcium carbonate material, we selected a mollusk shell from the same sample interval as foraminiferal tests for radiocarbon dating (0.05 m depth). The foraminifera provided an older age of 1,753 ± 143 cal yr B.P. than the mollusk shell, which was dated to 589 ± 97 cal yr B.P. The difference in the ages may be the result of multiple processes: an amalgamation of material in a condensed section on the sediment-starved modern shelf; the presence of sediments containing detrital carbonate within the foram tests resulting in an older age; or perhaps diagenetic alteration of the foram tests, with recrystallization of pore water carbonate incorporating older material on the foraminifer tests, which have a higher surface area to mass ratio than the mollusk shells. Regardless, both ages indicate a much younger age for the 14 cm thick open shelf deposit (Figure 11C) than any of the estuary sediments in the river valley. Seismic data at this location show prominent draping of sediments along the edges of the terrace (Figure 11A), and a spike in fragmentation of foram tests coincides with the contact between the terrace and modern deposition (0.14 m depth), indicating a more significant amount of reworking at the contact.

4.6 *Gravity core 2*

GC-2's location was chosen to identify a set of dipping reflectors believed to be part of a tidal delta (Figure 12A). The core consists primarily of medium-gray clayey-silt with numerous layers of silty sand (Figure 12). The lower part of the core (~2.0-3.6 m depth) contains foraminifera approximating 50-50 *Ammonia* and *Elphidium*. This assemblage combined with the

EarthArXiv preprint – this manuscript is not peer reviewed

increased sand content and the relatively higher percent of foram test fragmentation indicate this section likely contains tidal delta deposits. Because it is capped by a less-sandy section dominated by *Elphidium* indicating an outer bay environment (~0.4-2.0 m depth), the base of the core is interpreted as a flood-tidal delta. Carbon dates from mollusk shells obtained near the transition from tidal delta to outer bay at 2.07 m depth and 2.19 m depth provide ages of 8,445 ± 135 cal yr B.P. and 8,546 ± 173 cal yr B.P., respectively. The top of the core (0.4 m depth) contains a spike in *Ammonia* coupled with an increase in fragmentation. Similar to GC-5, coincident increase in fragmentation with a spike in *Ammonia* likely represents a reworking of central bay material in the outer bay environment. The transition to modern inner shelf deposition begins at ~0.5 m depth (~7.0 ka), represented by the increase in foraminiferal diversity and presence of agglutinated foraminifera.

5. Discussion

The coring locations in this study were chosen to sample specific seismic facies and were not intended to provide a cross-section down the Holocene estuary. However, the data can provide several short cross sections along strike in the proximal, middle, and distal parts of our study area generating a composite picture of the nature and timing of environmental change across this part of the estuary from its initial flooding ~10 ka to its continued evolution by ~6 ka. An analysis of the cores across the incised valley combined with interpolated ages from the age models shows consistent paleoenvironmental changes across multiple cores (Figure 13), some of which coincide with events along the Texas Gulf Coast (Figure 14; e.g., Anderson et al., 2022; 2016; Anderson and Rodriguez, 2008; Simms et al., 2010; Troiani et al., 2011). The most

landward part of this cross-section (Figure 13, A-A'; Figures 5 & 6) shows that PC-2 and PC-4 both transition from fluvial/terrestrial environments to upper bay at the same time (~9.8 ka); however, the extrapolated age model date for PC-4 is not conclusive that the transition occurred simultaneously at both locations. Additionally, PC-2 and PC-4 do not transition from upper bay to central bay environments at the same time (PC-2 at ~9.6 ka and PC-4 at ~8.8 ka), likely due to the elevation of the Pleistocene terrace at PC-4's location. Subsequent environmental changes along this profile appear to occur simultaneously. PC-2, PC-4, and GC-6 all transition from central bay to outer bay environments at approximately the same time – 8.2-8.0 ka. Similarly, GC-2 (Figure 13, C-C') and GC-5 (Figure 13, B-B') show a coincident transition to outer bay environment at ~8.4 ka; however, GC-4 does not transition to an outer bay environment until ~7.9 ka. In general, outer bay sediments show a seaward thickening sequence from PC-2's location (Figure 13, D-D').

Additionally, all cores in the study area, except for GC-6, appear to transition to an inner shelf environment beginning at ~6.9 ka. Although this interval is difficult to date because of erosion of material during transgression and the limited inner shelf sediments observed in all cores (Figure 14C), coincident timing suggests that the paleoestuary was relatively stable and changes in shoreline position and/or lateral shifts in the position of the tidal inlet led to the observed environmental transitions. Overall, the lateral differences in sediments within the cores reflect contemporaneous estuarine environmental variability.

Micropaleontologic evidence from these cores confirms the existence of a long-term stable estuarine environment; however, the seaward boundary of this estuary is not well-constrained with the existing dataset (Figure 15), and further research on the seaward side of

our study area is needed to determine when and where this boundary shifted. Approximately 9.8-9.6 ka, a large estuary stretched from the modern shoreline of Galveston Bay to seaward of Heald Bank (Figure 15a). The flood-tidal delta at the base of GC-2 indicates that, in the vicinity of the Trinity River Paleovalley, the shoreline shifted landward of Heald Bank by at least 8.8 ka (Figure 15b). In particular, our data suggest the paleoestuary was present landward of Heald Bank for ~2 kyr (~8.8-6.9 ka) with some tidal inlet changes that altered the environment within the estuary without evidence of shoreline transgression (Figure 15a-c, Burstein et al., 2023). In contrast, Rodriguez et al. (2004) concluded that the shoreline was approximately at Heald Bank's location at ~7.7 ka. These apparently contradictory observations could be reconciled if, as Rodriguez et al. (2004) postulated for the 5.3 ka shoreline, the 7.7 ka shoreline also exhibited a significant bend or step (Figure 15d). While such a geometry may seem unrealistic, the southern end of Assateague Island and its transition to Wallops Island, on the Eastern Shore of Virginia on the US Atlantic Coast, is a possible modern analog for such a formation.

Although we have mapped the estuarine sediments within the bounds of the Trinity River incised paleovalley (Figure 15), it is possible that the estuary extended beyond the paleovalley, just as it does in the modern setting, and any estuarine sediments to the east and west of our study area have been removed during transgressive erosion. A subsequent landward shift took place ~6.9 ka when the barrier system transgressed to a location between GC-2 and GC-5 (Figure 15d). This shift was followed by additional landward barrier migration. The age of this later transgression cannot be determined in our cores because of the erosion of material as the shoreline passed across our study area. Transgressive lag deposits in GC-6 combined with overlying inner shelf environment of the cores, indicate the shoreline was

548 landward of our study area by at least 4.3 ka (Figure 15e-f). This is consistent with previous
549 studies (e.g., Anderson et al., 2008; Rodriguez et al., 2004), which, based on radiocarbon dating
550 of beach ridges, conclude that the shoreline reached its modern location on Galveston Island by
551 ~5.3 ka on the western side (15e-f) (Anderson et al., 2022; Rodriguez et al., 2005).
552
553 5.1 *Stable paleoestuary*
554 Extensive research conducted by the Anderson group argues for the existence of >75 km
555 long paleoestuary from Heald Bank ~50 km offshore Galveston Bay to the modern bay between
556 ~8.2-7.8 ka (Figure 3) (Anderson et al., 2008; Rodriguez et al., 2004). This evidence includes
557 seismic data and carbon dating of sediment cores from within modern Galveston Bay and Heald
558 Bank (Anderson et al., 2008; Rodriguez et al., 2004).
559 Foraminiferal analysis from PC-2 and PC-4 indicates that both sites were located in the
560 central bay from at least 8.8 ka to 8.0 ka, although PC-2 transitioned to a central bay
561 environment by ~9.6 ka, confirming the existence of a long-term stable estuary (Figures 5 & 6).
562 Foraminiferal assemblages in PC-2 and PC-4 during this time period were dominated by
563 *Ammonia* with common *Elphidium*, corresponding to a central bay depositional environment.
564 Assemblages in PC-4 moving up through the core (2.7-1.3 m depth) show a decreasing
565 abundance of *Ammonia* and an increase in *Elphidium* over time indicating a gradual
566 environmental transition from upper bay to central bay and to outer bay. However, higher
567 resolution analysis of PC-2 shows fluctuations in *Ammonia* and *Elphidium* abundances
568 throughout the entire central bay interval, which may correspond to salinity fluctuations within
569 the Holocene estuary as tidal inlets changed shape and/or location, or perhaps as precipitation

EarthArXiv preprint – this manuscript is not peer reviewed

in the catchment varied. This suggests that although environmental variability occurred within the paleoestuary, the outer boundaries remained stable enough to maintain a central bay environment. Additionally, many of the peaks in *Ammonia* correspond to small increases in foram fragmentation (e.g., 3.4 and 3.7 m depth), which may indicate reworking of central bay material during that interval. The PC-2 analysis shows that portions of the estuary experienced marine mixing at ~8.4 ka (Figure 5B) coinciding with a transition of seaward core locations to outer bay environments (Figure 13, B-B' & C-C'). Increased marine influence on the estuary may provide an explanation for the small variations in foraminiferal assemblages observed in the middle estuary. Despite these marine incursions, the paleoestuary was likely protected due to the formation of barrier islands in the paleovalley (Burstein et al., 2023).

GC-4 is located at the western edge of the paleovalley and contains sediment and foraminiferal assemblages that record lateral variation in the boundary of the estuary between ~8.2 ka and ~8.1 ka (Figure 9 and 13). While it is difficult to pinpoint the exact forcing mechanism for this expansion with existing evidence, it coincided with an environmental transition in GC-6. This suggests that the western boundary of the paleoestuary expanded due to sea level rise prior to probable partial barrier collapse/rollover and the transition to an outer bay seen first in GC-6 and subsequently in PC-2 and PC-4 (Figure 13). Although this expansion may have impacted the stability of the barrier system, it is unlikely that the shoreline changed significantly based on the maintenance of an outer bay environment during this time at GC-2's location (Figure 12) and the existence of tidal delta deposits identified by Thomas and Anderson (1994) (Figure 15). High-resolution seismic data in our study area show that antecedent fluvial

EarthArXiv preprint – this manuscript is not peer reviewed

highs probably provided a pinning point for the barrier system to stabilize at, which likely protected the paleoestuary during periods of rapid sea level rise (Burstein et al., 2023).

5.2 *Paleoshoreline changes*

Rodriguez et al. (2004) describe estuarine muds in Heald Bank cores that were dated to 8,015 ± 50 and 7,770 ± 65 yr ago (both from articulated *Mulinia lateralis* bivalves) and suggested that the paleoshoreline was at Heald Bank ~7.77 ka. Due to the limited preservation of barrier islands offshore in the sediment record, we must infer original island locations or areas of development based on the sediments that are preserved. Tidal inlet and tidal delta deposits are considered evidence for the presence of barrier systems that are not preserved (Anderson et al., 2016). Analysis of GC-2 reveals the existence of flood tide delta deposits dated to before ~8.5 ka, indicating that the inlet (and thus the barrier island system) was nearby (Figure 12) (Burstein et al., 2023). Likewise, the presence of sandy deposits in GC-5 at ~6.7 ka and GC-6 at ~4.3 ka potentially demonstrates the landward migration of the paleoshoreline as sea level continued to rise throughout the Holocene (Figure 16). Both GC-2 and GC-5 transition to outer bay environments by ~8.4 ka (Figures 10 & 12), indicating that the outer boundary of the estuary within the Trinity River Paleovalley shifted and/or the paleobarrier system collapsed/rolled over prior to the transition to what are described as sandy shoreface deposits in Heald Bank cores (Rodriguez et al., 2004). As noted above, these observations could be reconciled if, as Rodriguez et al. (2004) postulated for the 5.3 ka shoreline, the 7.7 ka shoreline also exhibited a significant bend or step (Figure 15d).

EarthArXiv preprint – this manuscript is not peer reviewed

Sandy deposits in the outer bay sequence of GC-5 are probable washover sediments from a proximal barrier island. The absence of these sands in the bay margin intervals of GC-4 (Figure 9) indicate that these washovers are not from the edge of the bay, westward of GC-5's location (Figure 10 & 13). We hypothesize that a barrier system developed near GC-5's position ~20 km seaward of the modern shoreline ~6.7 ka (Figure 15). Sandy intervals in the outer bay section of GC-2, located seaward of GC-5, containing a shell with an age of 6,973 ± 170 cal yr B.P. also suggest that a barrier had developed nearby in the seaward direction, and these sandy intervals could represent paleo-storm/washover deposits from that barrier system.

In addition to the data provided in GC-2 and GC-5, transgressive lag deposits in GC-6 (Figure 7) suggest that there was a barrier system proximal to GC-6's location between ~7.4 and 4.3 ka (Figure 15). The upper sample obtained from GC-6 closely resembles a modern marsh assemblage from Galveston Island (see 4.3), indicating that these sandy deposits could be from either a back-barrier marsh or a marsh located on the edge of the paleoestuary, and are not remnant ebb-tidal delta deposits (Figure 8). Although we cannot confirm the timing and location of a paleobarrier near GC-6 with our current dataset, the foraminiferal assemblage identified at the top of the sandy sediments can only be explained as originating from a back-barrier marsh. Additionally, the lack of organic material in the sandy sediments suggests that these sediments are not from a relict barrier island but have been reworked from a backbarrier marsh environment.

Analysis of Galveston Island core data by Rodriguez et al. (2004), coupled with previous research on the island by Bernard et al. (1970), indicates that Galveston Island began prograding ~5.3 ka giving the paleoshoreline an irregular shape and showing rapid, rather than gradual,

coastline changes in the past (Figure 2 & 15). Although coastal changes typically adjust to sea level rise "dynamically while maintaining a characteristic geometry that is unique to a particular coast" (FitzGerald et al., 2008, p. 601), it is likely the irregular depth of the Holocene-Pleistocene surface on either side of the Trinity River paleovalley (Figure 2) is the cause for this oblique paleoshoreline change (Rodriguez et al., 2004). Based on probable washover and transgressive lag sediments reported here, the paleoshoreline east of Galveston Island's location likely stepped landward multiple times until reaching is modern-day location by ~2.5 ka; however, the lack of data between our study area and the modern shoreline makes it difficult to constrain this migration beyond the proximity of the shoreline to GC-6 at ~4.3 ka.

5.3 *Timeline of sea level rise*

Estimates of Antarctic ice-sheet fluctuations since the Last Glacial Maximum vary widely, so most Holocene sea level rise is attributed to the better constrained demise of the Laurentide Ice Sheet (Lambeck et al., 2014); however, initial retreat of the West Antarctic and Antarctic Peninsula Ice Sheets began between 15.0 and 12.0 ka with significant retreat in the Ross and possibly Weddell Seas after 7.0 ka (Anderson et al., 2002) and a more recent synthesis of Antarctic Holocene deglaciation indicates that a majority of melting occurred by or shortly after 5 ka (Bentley et al., 2014). Higher resolution analysis of Laurentide Ice Sheet deglaciation reveals multiple meltwater pulses at 9.1 ka, 8.7 ka, 8.6 ka, 8.2 ka, and 7.4 ka (Cronin et al., 2007; Jennings et al., 2015; Törnqvist et al., 2004; Ullman et al., 2016). After 8.15 ka, Laurentide Ice Sheet retreat accelerated with remnant ice domes melting by ~6.7 ka (Lambeck et al., 2014;

Ullman et al., 2016). Remaining global sea level rise is attributed to the loss of ice volume from the West Antarctic ice-sheet during the late Holocene (Ullman et al., 2016).

While many of these pulses can be connected to rapid environmental change along the Gulf Coast, some events are more likely due to the impact of antecedent geology (Anderson et al., 2014; Burstein et al., 2023) and/or regional climate changes impacting sediment supply (Anderson and Rodriguez, 2008). A comparison of environmental changes in the paleoestuary and the record of Gulf of Mexico sea level rise indicates that most of these transitions coincide with or occurred after periods of rapid increases in sea level, although some environmental shifts transpired after global sea level rise slowed significantly, indicating other regional and local changes, such as hydroclimate, may have contributed to these transitions (Figure 14).

Many of the environmental transitions in our study area correlate with flooding surfaces identified in other Gulf Coast bays, when the rate of sea level rise was 4.2 mm yr^{-1}, suggesting global sea level rise played a dominant role. At 9.8 ka, PC-2 transitions from a fluvial to an upper bay environment. Inundation in the Galveston paleoestuary also coincides with the initial flooding of the Sabine-Neches incised valley (Milliken et al., 2008c) and a flooding surface in Matagorda/Lavaca estuary complex (Maddox et al., 2008). At ~9.6 ka, the estuarine setting at core site PC-2 transitioned from an upper bay to central bay environment (Figure 5 & 14), shortly after flooding in the modern Galveston Bay that resulted in formation of a bayhead delta (Anderson et al., 2008). This generally coincided with initial flooding of Copano Bay (Troiani et al., 2011), and the landward stepping of the fluvial system in Sabine Lake (Milliken et al., 2008b). A drowning event of the Nueces River valley in Corpus Christi Bay at about this time may or may not have been a rapid flooding event (Simms et al., 2008). These events likely resulted from sea

level rise caused by the retreat of the Antarctic Ice Sheet (Anderson et al., 2002) and are either within or just after a period of rapid sea level rise identified by Milliken et al. (2008a). PC-4's location transitioned from an upper bay to central bay environment at ~8.8 ka, coinciding with a period of rapid sea level rise (Milliken et al., 2008a) and a flooding event in Calcasieu Lake that shifted the bay shoreline landward (Milliken et al., 2008b) and shortly after flooding events in modern Galveston Bay (Anderson et al., 2008) and Corpus Christi Bay (Simms et al., 2008). The lack of longer cores in the seaward portion of our study area precludes our ability to determine if the outer boundary of the estuary shifted along with the paleoenvironmental changes at PC-2 and PC-4; however, previous analysis suggests that the paleoshoreline likely did not shift landward until barrier migration ~6.9 ka (Burstein et al., 2023).

There are a series of paleoenvironmental changes between 8.5 and 7.9 ka, likely in response to rapid sea level rise events, in which the paleoestuary progressively transitions from a central bay to an outer bay environment. These changes partially coincide with a significant deglacial event, typically referred to as the "8.2 ka event," in which a large glacial lake drained into the North Atlantic and led to short-term climate cooling (Cronin et al., 2007; Jennings et al., 2015; Törnqvist et al., 2004; Ullman et al., 2016). Other portions of the Texas Gulf Coast also experienced rapid flooding events likely as a result of global pulses of sea level rise, including Matagorda/Lavaca estuary complex (~8.5-8.2 ka; Maddox et al., 2008), Copano Bay (~8.2 ka, Troiani et al., 2011), Baffin Bay (~8.0 ka, Simms et al., 2010), Mobile Bay (~8.7-8.2 ka; Rodriguez et al., 2008b), Sabine Lake (~8.4-8.0 ka; Milliken et al., 2008c), Calcasieu Lake (~8.3-8.0 ka; Milliken et al., 2008b), modern Galveston Bay (~8.2 ka; Anderson et al., 2008), and Corpus Christi Bay (~8.0 ka; Simms et al., 2008). There is also an increase in diversity of the foraminiferal

699 population in PC-2 between 8.4 and 8.1 ka, possibly due to elevated salinity levels from a partial
700 or total collapse/rollover of the barrier system as other portions of the paleoestuary
701 transitioned more saline environments (Figure 5). This also corresponds to the 8.2 ka flooding
702 event observed elsewhere. Additionally, carbon isotope records show that between 11.0 and
703 8.0 ka, the central Texas region was transitioning to a warmer and drier climate (Nordt et al.,
704 2002, 1994), so it is likely that the drying hydroclimate reduced sediment supply, which
705 contributed to these changes.

706 Slightly before 8.5 ka, foraminiferal populations within GC-2 (the most seaward core in
707 our study area) exhibit an increase in inner shelf species (Figure 12), suggesting a marine
708 incursion at that location and the beginning of a landward migration of the Galveston
709 paleoestuary. This is followed by a transition at ~8.5 ka in GC-2 from a flood-tidal delta
710 environment to an outer bay environment, potentially demonstrating a stabilization in the
711 barrier system (Figure 12). At 8.4 ka, GC-5 transitioned to outer bay environments (Figure 10),
712 coinciding with landward migration of the river mouth in the Matagorda/Lavaca estuary
713 complex (Maddox et al., 2008), rapid (~100 m yr^{-1}) landward transgression of the bayline in
714 Mobile Bay (Rodriguez et al., 2008b), and landward movement of the bayline in Sabine Lake
715 (Milliken et al., 2008c). At 8.3 ka, sediments in GC-4 transition from a bay margin to a central
716 bay environment (Figure 9 & 14), interpreted as a sea level rise event that expanded the
717 boundaries of the paleoestuary. In addition to the above flooding events at ~8.4 ka, the GC-4
718 transition also coincided with a landward shift in the bayhead delta in Calcasieu Lake (Milliken et
719 al., 2008b). At ~8.2 ka, within modern Galveston Bay, the bayline shifted ~10 km up the valley
720 along with the landward migration of the bayhead delta (Anderson et al., 2008). Within our

721 study area, the Galveston paleoestuary boundaries contracted ~8.1 ka and GC-6's location
722 transitioned to an outer bay environment (Figure 7). By ~8.0 ka PC-2 and PC-4 both transitioned
723 to an outer bay environment (Figure 5 & 6), coincident with a rapid flooding event in Corpus
724 Christi Bay in which the upper bay backstepped by 15 km in <200 yr and much of the modern
725 bay became an open bay environment (Simms et al., 2008). Within the Galveston paleoestuary,
726 GC-4 transitioned to an outer bay environment at ~7.9 ka (Figure 9). Other changes along the
727 Texas Gulf Coast include a landward shift of the delta within the Matagorda/Lavaca estuary
728 complex between 7.9-7.7 ka and an expansion of Lavaca Bay followed by spit formation
729 (Maddox et al., 2008), and a 10-km backstepping of the delta landward within Calcasieu Lake
730 (Milliken et al., 2008b).
731 By 7.8 ka, all cores within our study area had transitioned to outer bay (Figure 14). This
732 was followed by an increase in inner shelf species within foraminiferal populations at PC-4
733 suggesting more marine conditions at that location (Figure 5), a 10-20 km landward movement
734 of the bayline in Sabine Lake (Milliken et al., 2008c), and initial flooding of the estuary in Weeks
735 Bay (Rodriguez et al., 2008a). Although there are no changes within our study area between 7.7-
736 7.4 ka, it is worth noting that sediments in the modern Galveston Bay show a flooding surface
737 constrained to this time (Figure 3) and landward migration of the bayhead delta and central bay
738 (Anderson et al., 2008).
739 At ~7.3 ka, shortly after a deglacial event and a regional climate shift to warmer and
740 drier conditions, there is a brief increase in diversity in foraminiferal populations in GC-5 (Figure
741 10), possibly associated with increased marine mixing, although there are no other indications
742 of environmental change in other cores. This coincides with a dramatic change in the

743 Matagorda/Lavaca estuary complex in which the bayhead delta shifted by 30 km between 7.3
744 and 6.7 ka, establishing the modern-day Matagorda Bay (Maddox et al., 2008).

745 After 7.0 ka, sea level rise slowed to 1.4 mm yr^{-1} and the paleoestuary appears to have
746 stabilized until marine transgression sometime between 6.7 ka and ~4.3 ka, although that is
747 difficult to pinpoint due to removal of material. The approximate timing of the transgressive
748 ravinement overlaps with flooding surfaces in Sabine Lake (Milliken et al., 2008c), Calcasieu Lake
749 (Milliken et al., 2008b), and Corpus Christi Bay (Simms et al., 2008). It is likely that a central
750 Texas regional climate change from cool/wet to warm/dry conditions by ~8.0 ka with peak
751 warm/dry conditions around ~6.0 ka (Figure 14; Bryant and Holloway, 1985; Nordt et al., 2002,
752 1994) contributed to these changes by reducing the sediment supply to the paleoestuary
753 allowing for the landward migration of the paleoshoreline (Figure 15). By ~5 ka, Antarctic ice
754 sheet melting was mostly complete (Bentley et al., 2014), after which our study environment
755 stabilized as an inner shelf/open marine environment.

756 The influence of regional climate change, particularly hydroclimate, on paleoestuary
757 stability suggests that modern warming, especially in combination with reduced precipitation,
758 coupled with human-induced reduction in riverine sediment flux and subsidence may increase
759 the vulnerability of Galveston Island and Bolivar Peninsula to accelerating sea level rise. We are
760 unable to determine the magnitude of change in sediment flux that resulted in previous
761 shoreline retreat, as the only indication of this change is the mid-Holocene transition from a
762 wet/cool to a warm/dry hydroclimate ~7.4 ka and to a more variable climate ~4 ka likely when
763 our study area became inner shelf and the paleoshoreline was still in the process of migrating to
764 its modern-day location (Figure 14 & 15; Weight et al., 2011). Foraminiferal data indicates there

765 were fluctuations in the estuarine environment while the shoreline was stable, suggesting
766 alterations to salinity that may be due to hydroclimate changes or increased marine mixing from
767 inlet changes. Additional study is required involving paleoclimate and paleoprecipitation
768 changes in the Trinity River catchment to deduce how changes in sediment supply to the coast
769 may have contributed to Holocene coastal change.
770
771 5.4 *Minimal modern seafloor sedimentation*
772 The transition to a modern inner shelf environment is difficult to determine due to the
773 limited amount of modern seafloor material and likely erosion and reworking of upper
774 sediments from the transgressive ravinement. The only indication of the timing of transgression
775 through our study area are radiocarbon dates of ~6.9 ka in GC-2 and ~6.7 ka in GC-5 prior to the
776 transition from outer bay to inner shelf, and the transgressive lag deposit in GC-6 containing a
777 radiocarbon dated shell of ~4.3 ka (Figures 13-15). Based on these dates, it is likely that the
778 transgression in our study area occurred over the period between 7.0 and 6.0 ka. The limited
779 shelf material in the upper areas of each core represents deposition of ~0.01 cm per year, so it
780 is more likely that material is being removed from the upper seafloor regularly.
781 The Texas Mud Blanket is a large (~300 km^3) depositional area on the western Gulf Coast
782 between a bathymetric embayment of the ancient Rio Grande and Colorado River deltas
783 containing ~$5x10^{11}$ t of sediment (Weight et al., 2011). It is likely that depletion of inner shelf
784 sediments offshore Galveston Bay is the result of sediment remobilization via the Louisiana-
785 Texas Coastal Current to regions farther west along the Texas Coast, including the Texas Mud
786 Blanket.

EarthArXiv preprint – this manuscript is not peer reviewed

6. Conclusion

We use new cores to refine the established Holocene coastal change model for the Trinity River incised valley based on new radiocarbon dates and micropaleontological analysis. This study provides environmental context to previous research that primarily utilized seismic and sedimentological analyses, revealing consistent environmental changes across multiple cores due to external sea level rise and climate forcing. As a result of this analysis, we reach the following conclusions:

- Despite periods of rapid sea level rise, the Galveston paleoestuary was relatively stable for approximately 2 kyr (~8.8-6.9 ka) and experienced gradual environmental shifts within the paleoestuary associated with rapid sea level rise events (e.g., the 8.2 ka event). Our data show that the paleoestuary experienced marine incursions and probable tidal-inlet migrations in otherwise stable outer boundaries that altered the paleoenvironment within the bay but did not collapse the paleoestuary entirely prior to full migration and marine transgression.
- Probable washover sediments approximate the location of barrier islands as they migrated landward at ~7-6.7 ka and after ~4.3 ka. Data limitations preclude our ability to characterize how the barrier system may have migrated landward of our study area; however, based on previous analysis, the western side of the paleovalley was near its modern location by ~5.3 ka and the eastern side migrated to its current location by ~2.5 ka.

- Early Holocene paleoenvironmental changes coincide with previously identified flooding events in other Gulf Coast bays, suggesting global sea level rise was a dominant cause of these changes. Subsequent middle to late Holocene paleoenvironmental transitions during reduced rates of sea level rise were likely caused by regional hydroclimate change to warm and dry conditions that reduced sediment supply to the coast.
- All cores in the study area contain minimal modern seafloor sediments likely due to erosion from the transgressive ravinement and re-working of sediment from ocean currents contributing to the Texas Mud Blanket.

7. Data Availability

Datasets related to this article can be found at https://www.ncei.noaa.gov/access/paleo-search/study/34592, an open-source online data repository hosted at NOAA's National Center for Environmental Information.

Conflict of Interest

The authors declare no conflict of interest.

8. Acknowledgments

This project was funded by the Bureau of Ocean Energy Management under Cooperative Agreement M16AC00020, and the Martin B. Lagoe Micropaleontology Fellowship from the Jackson School of Geosciences at the University of Texas at Austin. We would like to thank Gabriela Gutierrez, Daniel Duncan, Marcy Davis, the crew of the R/V *Brooks McCall*, TDI Brooks,

the class of the 2018 Marine Geology and Geophysics Field Course, and the crew of the R/V *Manta* for their collective assistance in collecting the piston and gravity cores and additional chirp data for this study, and Nikki Bretting and Kate Gilbreath for assistance in grain size analysis. We would also like to thank the National Ocean Sciences Accelerator Mass Spectrometry at Woods Hole Oceanographic Institute (NSF Cooperative Agreement number OCE-0753487) for processing our radiocarbon samples, and the Gulf of Mexico Sedimentology Working Group for discussions contributing to the analysis presented in this paper. We acknowledge that research on this project was conducted at the University of Texas at Austin on the Indigenous lands of Turtle Island, on land originally cared for by the Alabama-Coushatta, Caddo, Carrizo/Comecrudo, Coahuiltecan, Comanche, Kickapoo, Lipan Apache, Tonkawa, and Ysleta del Sur Pueblo people, many of whom were forcibly removed from their home. For more information about ancestral land you occupy, please visit https://native-land.ca/. This is University of Texas Institute for Geophysics Contribution #XXXX.

Tables

Table 1. List of radiocarbon dating samples and their calibrated ages.

No.	NOSAMS OS No.	Sample	Type	Process	Calibrated Age	
					Age (yr)	Error (± yr)
1	155814	PC-2-S3-7-8.5	Mollusk	Hydrolysis	7,441	127
2	152146	PC-2-S3-82-83.5	Mollusk	Hydrolysis	7,800	134
3	152138	PC-2-S2-69.5-71	Mollusk	Hydrolysis	8,468	135

4	152145	PC-2-S2-100.5-102	Mollusk	Hydrolysis	8,815	175
5	155815	PC-2-S1-14-16	Mollusk	Hydrolysis	9380	133
6	155816	PC-2-S1-23-25	Mollusk	Hydrolysis	9,420	124
7	155817	PC-2-S1-102-104	Mollusk	Hydrolysis	9,794	215
8	155818	PC-4-S3-58.5-60	Mollusk	Hydrolysis	7,787	136
9	152148	PC-4-S3-59	Mollusk	Hydrolysis	41,030	1,703
10	155819	PC-4-S2-15-16.5	Mollusk	Hydrolysis	8,815	175
11	152147	PC-4-S2-94-96	Mollusk	Hydrolysis	9,131	158
12	155820	GC-1-S1-4-6	Foraminifera (*Ammonia, Elphidium, Bolivina,* and *Bulimina*)	Hydrolysis	1,753	143
13	152314	GC-1-S1-5-6	Mollusk	Hydrolysis	589	97
14	152315	GC-1-S1-28.5-30	(*Ammonia* and *Elphidium*)	Hydrolysis	38,081	1,833
15	155821	GC-2-S1-A-59-61	Mollusk	Hydrolysis	6,973	170
16	152310	GC-2-S2-144-145	Mollusk	Hydrolysis	8,445	135
17	152316	GC-2-S3-6-10	Mollusk	Hydrolysis	8,546	173
18	155902	GC-4-S1-55.5-56.5	plant fragments	Combustion	7,913	255
19	152149	GC-4-S2-13-13.5	plant fragments	Combustion	7,977	221
20	155903	GC-4-S3-120-122	plant fragments	Combustion	8,470	144

21	155822	GC-5-S2-3-5	Mollusk	Hydrolysis	6,661	169
22	155823	GC-5-S3-32-37.5	Mollusk	Hydrolysis	8,445	135
23	155824	GC-5-S3-74-76	Mollusk	Hydrolysis	8,467	130
24	155825	GC-6-S1-11-14	Mollusk	Hydrolysis	>Modern	
25	155826	GC-6-S1-64.5-66	Mollusk	Hydrolysis	4,329	165
26	157505	GC-6-S1-111.5-113	Mollusk	Hydrolysis	7,760	142
27	157506	GC-6-S1-130-131.5	Mollusk	Hydrolysis	7,709	147
28	157511	GC-6-S2-71-72.5	Mollusk	Hydrolysis	8,367	181

9. References

Abdulah, K.C., Anderson, J.B., Snow, J.N., Holdford-Jack, L., 2004. The Late Quaternary Brazos and Colorado Deltas, Offshore Texas, U.S.A.—Their Evolution and the Factors that Controlled Their Deposition.

Anderson, J.B., Rodriguez, A.B., 2008. Response of Upper Gulf Coast Estuaries to Holocene Climate Change and Sea level Rise. Geological Society of America.

Anderson, J.B., Rodriguez, A.B., Milliken, K.T., Taviani, M., 2008. The Holocene evolution of the Galveston estuary complex, Texas: Evidence for rapid change in estuarine environments, in: Special Paper 443: Response of Upper Gulf Coast Estuaries to Holocene Climate Change and Sea level Rise. Geological Society of America, pp. 89–104. https://doi.org/10.1130/2008.2443(06)

Anderson, J.B., Wallace, D.J., Rodriguez, A.B., Simms, A.R., Milliken, K.T., 2022. Holocene Evolution of the Western Louisiana–Texas Coast, USA: Response to Sea level Rise and Climate Change, in: Anderson, J.B., Wallace, D.J., Rodriguez, A.B., Simms, A.R., Milliken, K.T. (Eds.),

862 Holocene Evolution of the Western Louisiana–Texas Coast, USA: Response to Sea level Rise
863 and Climate Change. Geological Society of America. https://doi.org/10.1130/2022.1221(01)
864 Anderson, J.B., Wallace, D.J., Simms, A.R., Rodriguez, A.B., Milliken, K.T., 2014. Variable response
865 of coastal environments of the northwestern Gulf of Mexico to sea level rise and climate
866 change: Implications for future change. Marine Geology 352, 348–366.
867 Anderson, J.B., Wallace, D.J., Simms, A.R., Rodriguez, A.B., Weight, R.W.R., Taha, Z.P., 2016.
868 Recycling sediments between sourece and sink during a eustatic cycle: Systems of late
869 Quaternary northwestern Gulf of Mexico Basin. Earth-Science Reviews 153, 111–138.
870 Bernard, H.A., Major, C.F., Parrott, B.S., LeBlanc, R.J., 1970. Recent sediments of southeast
871 Texas-a field guide to the Brazos alluvial and deltaic plains and the Galveston barrier island
872 complex. University of Texas at Austin, Bureau of Economic Geology.
873 Bernstein, A., Gustafson, M.T., Lewis, R., 2019. Disaster on the horizon: The price effect of sea
874 level rise. Journal of Financial Economics 134, 253–272.
875 https://doi.org/10.1016/j.jfineco.2019.03.013
876 Blaauw, M., Christen, J.A., 2011. Flexible paleoclimate age-depth models using an
877 autoregressive gamma process. Bayesian Anal. 6, 457–474. https://doi.org/10.1214/11-
878 BA618
879 Bratton, J.F., Colman, S.M., Thieler, E.R., Seal, R.R., 2002. Birth of the modern Chesapeake Bay
880 estuary between 7.4 and 8.2 ka and implications for global sea level rise. Geo-Mar Lett 22,
881 188–197. https://doi.org/10.1007/s00367-002-0112-z
882 Bryant, V., Holloway, R., 1985. A late-Quaternary paleoenvironmental record for Texas: an
883 overview of the pollen evidence. Pollen records of late-Quaternary North American
884 sediments 39–70.
885 Burstein, J.T., Goff, J.A., Gulick, S.P.S., Lowery, C., Standring, P., Swartz, J., 2023. Tracking barrier
886 island response to early Holocene sea level rise: High resolution study of estuarine sediments
887 in the Trinity River Paleovalley. Marine Geology 106951.
888 https://doi.org/10.1016/j.margeo.2022.106951
889 Buzas, M.A., 1990. Another look at confidence limits for species proportions. Journal of
890 Paleontology 2.

Buzas-Stephens, P., Livsey, D.N., Simms, A.R., Buzas, M.A., 2014. Estuarine foraminifera record Holocene stratigraphic changes and Holocene climate changes in ENSO and the North American monsoon: Baffin Bay, Texas. Palaeogeography, Palaeoclimatology, Palaeoecology 404, 44–56. https://doi.org/10.1016/j.palaeo.2014.03.031

Cronin, T.M., Vogt, P.R., Willard, D.A., Thunell, R., Halka, J., Berke, M., Pohlman, J., 2007. Rapid sea level rise and ice sheet response to 8,200-year climate event. Geophysical Research Letters 34. https://doi.org/10.1029/2007GL031318

Culver, S.J., 1988. New Foraminiferal Depth Zonation of the Northwestern Gulf of Mexico. PALAIOS 3, 69–85. https://doi.org/10.2307/3514545

Culver, S.J., Woo, H.J., Oertel, G.F., Buzas, M.A., 1996. Foraminifera of coastal depositional environments, Virginia, U.S.A.; distribution and taphonomy. PALAIOS 11, 459–486. https://doi.org/10.2307/3515213

Davis, R.A., Hayes, M.O., 1984. What is a Wave-Dominated Coast?, in: Greenwood, B., Davis, R. A. (Eds.), Developments in Sedimentology, Hydrodynamics and Sedimentation in Wave-Dominated Coastal Environments. Elsevier, pp. 313–329. https://doi.org/10.1016/S0070-4571(08)70152-3

Dellapenna, T.M., Cardenas, A., Johnson, K., Flocks, J., 2009. Report of the Sand Source Investigation of the Paleo-Sabine-Trinity Marine Features. BOEM.

FitzGerald, D.M., Fenster, M.S., Argow, B.A., Buynevich, I.V., 2008. Coastal Impacts Due to Sea level Rise. Annual Review of Earth and Planetary Sciences 36, 601–647. https://doi.org/10.1146/annurev.earth.35.031306.140139

Forcino, F.L., Leighton, L.R., Twerdy, P., Cahill, J.F., 2015. Reexamining Sample Size Requirements for Multivariate, Abundance-Based Community Research: When Resources are Limited, the Research Does Not Have to Be. PLOS ONE 10, e0128379. https://doi.org/10.1371/journal.pone.0128379

Garrett, E., Brain, M.J., Hayward, B.W., Newnham, R., Morey, C.J., Gehrels, W.R., 2023. Resolving uncertainties in foraminifera-based relative sea level reconstruction: a case study from southern New Zealand. Journal of Foraminiferal Research.

Gehrels, W.R., 2013. Microfossil-Based Reconstruction of Holocene Relative Sea level Change. Sea Level Studies.

Goff, J.A., Allison, M.A., Gulick, S.P.S., 2010. Offshore transport of sediment during cyclonic storms: Hurricane Ike (2008), Texas Gulf Coast, USA. Geology 38, 351–354. https://doi.org/10.1130/G30632.1

Haslett, J., Parnell, A., 2008. A simple monotone process with application to radiocarbon-dated depth chronologies. Journal of the Royal Statistical Society: Series C (Applied Statistics) 57, 399–418. https://doi.org/10.1111/j.1467-9876.2008.00623.x

Hawkes, A.D., Horton, B.P., 2012. Sedimentary record of storm deposits from Hurricane Ike, Galveston and San Luis Islands, Texas. Geomorphology 171–172, 180–189. https://doi.org/10.1016/j.geomorph.2012.05.017

Heaton, T.J., Köhler, P., Butzin, M., Bard, E., Reimer, R.W., Austin, W.E.N., Ramsey, C.B., Grootes, P.M., Hughen, K.A., Kromer, B., Reimer, P.J., Adkins, J., Burke, A., Cook, M.S., Olsen, J., Skinner, L.C., 2020. Marine20—The Marine Radiocarbon Age Calibration Curve (0–55,000 cal BP). Radiocarbon 62, 779–820. https://doi.org/10.1017/RDC.2020.68

Jennings, A., Andrews, J., Pearce, C., Wilson, L., Ólfasdóttir, S., 2015. Detrital carbonate peaks on the Labrador shelf, a 13–7ka template for freshwater forcing from the Hudson Strait outlet of the Laurentide Ice Sheet into the subpolar gyre. Quaternary Science Reviews 107, 62–80. https://doi.org/10.1016/j.quascirev.2014.10.022

Kirwan, M.L., Megonigal, J.P., 2013. Tidal wetland stability in the face of human impacts and sea level rise. Nature 504, 53–60. https://doi.org/10.1038/nature12856

Lambeck, K., Rouby, H., Purcell, A., Sun, Y., Sambridge, M., 2014. Sea level and global ice volumes from the Last Glacial Maximum to the Holocene. PNAS 111, 15296–15303. https://doi.org/10.1073/pnas.1411762111

Leckie, R.M., Olson, H.C., 2003. Foraminifera as Proxies for Sea level Change on Siliciclastic Margins.

Maddox, J., Anderson, J.B., Milliken, K.T., Rodriguez, A.B., Dellapenna, T.M., Giosan, L., 2008. The Holocene evolution of the Matagorda and Lavaca estuary complex, Texas, USA, in: Anderson, J.B., Rodriguez, A.B. (Eds.), Response of Upper Gulf Coast Estuaries to Holocene Climate

948 Change and Sea level Rise. Geological Society of America, p. 0.
949 https://doi.org/10.1130/2008.2443(07)
950 Miller, M.M., Shirzaei, M., 2021. Assessment of Future Flood Hazards for Southeastern Texas:
951 Synthesizing Subsidence, Sea level Rise, and Storm Surge Scenarios. Geophysical Research
952 Letters 48, e2021GL092544. https://doi.org/10.1029/2021GL092544
953 Milliken, K.T., Anderson, J.B., Rodriguez, A.B., 2008a. A new composite Holocene sea level curve
954 for the northern Gulf of Mexico., in: Response of Upper Gulf Coast Estuaries to Holocene
955 Climate Change and Sea Level Rise, Geological Society of America Special Paper 443. pp. 1–
956 11.
957 Milliken, K.T, Anderson, J.B., Rodriguez, A.B., 2008b. Record of dramatic Holocene
958 environmental changes linked to eustasy and climate change in Calcasieu Lake, Louisiana,
959 USA, in: Anderson, J.B., Rodriguez, A.B. (Eds.), Response of Upper Gulf Coast Estuaries to
960 Holocene Climate Change and Sea level Rise. Geological Society of America, p. 0.
961 https://doi.org/10.1130/2008.2443(04)
962 Milliken, K.T, Anderson, J.B., Rodriguez, A.B., 2008c. Tracking the Holocene evolution of Sabine
963 Lake through the interplay of eustasy, antecedent topography, and sediment supply
964 variations, Texas and Louisiana, USA, in: Anderson, J.B., Rodriguez, A.B. (Eds.), Response of
965 Upper Gulf Coast Estuaries to Holocene Climate Change and Sea level Rise. Geological
966 Society of America, p. 0. https://doi.org/10.1130/2008.2443(05)
967 NOAA, 2023. Sea Level Trends, National Ocean and Atmospheric Administration.
968 https://tidesandcurrents.noaa.gov/sltrends/
969 Nordt, L.C., Boutton, T.W., Hallmark, C.T., Waters, M.R., 1994. Late Ouaternary Vegetation and
970 Climate Changes in Central Texas Based on the lsotopic Composition of Organic Carbon.
971 Quaternary Research 41, 109–120.
972 Nordt, L.C., Boutton, T.W., Jacob, J.S., Mandel, R.D., 2002. C4 Plant Productivity and Climate-CO2
973 Variations in South-Central Texas during the Late Quaternary. Quaternary Research 58, 182–
974 188. https://doi.org/10.1006/qres.2002.2344

975 Olson, H.C., Leckie, R.M. (Eds.), 2003. Micropaleontologic Proxies for Sea level Change and
976 Stratigraphic Discontinuities. SEPM (Society for Sedimentary Geology).
977 https://doi.org/10.2110/pec.03.75
978 Paine, J.G., 1993. Subsidence of the Texas coast: inferences from historical and late Pleistocene
979 sea levels. Tectonophysics, Geological Perspetives on Global Change 222, 445–458.
980 https://doi.org/10.1016/0040-1951(93)90363-O
981 Palermo, R.V., Piliouras, A., Swanson, T.E., Ashton, A.D., Mohrig, D., 2021. The effects of storms
982 and a transient sandy veneer on the interannual planform evolution a low-relief coastal cliff
983 and wave-cut platform at Sargent Beach, Texas, USA. Earth Surface Dynamics Discussions 1–
984 20.
985 Phleger, F.B., 1965. Patterns of Marsh Foraminifera, Galveston Bay, Texas. Limnology and
986 Oceanography 10, R169–R184. https://doi.org/10.4319/lo.1965.10.suppl2.r169
987 Phleger, F.B., 1960. Sedimentary Patterns of Microfaunas in Northern Gulf of Mexico1, in:
988 Shepard, F.P., Phleger, F.B., Andel, T.H.V. (Eds.), Recent Sediments, Northwest Gulf of Mexico.
989 American Association of Petroleum Geologists, p. 0. https://doi.org/10.1306/SV21353C10
990 Phleger, F.B., 1951. Ecology of Foraminifera, Northwest Gulf of Mexico. Geological Society of
991 America.
992 Poag, C.W., 2015. Benthic Foraminifera of the Gulf of Mexico: Distribution, Ecology,
993 Paleoecology. Texas A&M University Press.
994 Poag, C.W., 1981. Benthic Foraminifera of the Gulf of Mexico.
995 Ramsey, C.B., 2009. Bayesian Analysis of Radiocarbon Dates. Radiocarbon 51, 337–360.
996 https://doi.org/10.1017/S0033822200033865
997 Rehkemper, L.J., 1969. Sedimentology of Holocene Estuarine Deposits, Galveston Bay 12–52.
998 Reimer, P.J., Austin, W.E.N., Bard, E., Bayliss, A., Blackwell, P.G., Ramsey, C.B., Butzin, M., Cheng,
999 H., Edwards, R.L., Friedrich, M., Grootes, P.M., Guilderson, T.P., Hajdas, I., Heaton, T.J., Hogg,
1000 A.G., Hughen, K.A., Kromer, B., Manning, S.W., Muscheler, R., Palmer, J.G., Pearson, C., Plicht,
1001 J. van der, Reimer, R.W., Richards, D.A., Scott, E.M., Southon, J.R., Turney, C.S.M., Wacker, L.,
1002 Adolphi, F., Büntgen, U., Capano, M., Fahrni, S.M., Fogtmann-Schulz, A., Friedrich, R., Köhler,
1003 P., Kudsk, S., Miyake, F., Olsen, J., Reinig, F., Sakamoto, M., Sookdeo, A., Talamo, S., 2020. The

IntCal20 Northern Hemisphere Radiocarbon Age Calibration Curve (0–55 cal kBP). Radiocarbon 62, 725–757. https://doi.org/10.1017/RDC.2020.41

Rodriguez, A.B., 1999. Sedimentary facies and evolution of Late Pleistocene to recent coastal lithosomes on the east Texas shelf (Thesis).

Rodriguez, A.B., Anderson, J.B., Simms, A.R., 2005. Terrace Inundation as an Autocyclic Mechanism for Parasequence Formation: Galveston Estuary, Texas, U.S.A. Journal of Sedimentary Research 75, 608–620. https://doi.org/10.2110/jsr.2005.050

Rodriguez, A.B., Anderson, J.B., Siringan, F.P., Taviani, M., 2004. Holocene Evolution of the East Texas Coast and Inner Continental Shelf: Along-Strike Variability in Coastal Retreat Rates. Journal of Sedimentary Research 74, 405–421. https://doi.org/10.1306/092403740405

Rodriguez, A.B., Anderson, J.B., Siringan, F.P., Taviani, M., 1999. Sedimentary Facies and Genesis of Holocene Sand Banks on the East Texas Inner Continental Shelf. https://doi.org/10.2110/pec.99.64.0165

Rodriguez, A.B., Duran, D.M., Mattheus, C.R., Anderson, J.B., 2008a. Sediment accommodation control on estuarine evolution: An example from Weeks Bay, Alabama, USA, in: Anderson, J.B., Rodriguez, A.B. (Eds.), Response of Upper Gulf Coast Estuaries to Holocene Climate Change and Sea level Rise. Geological Society of America, p. 0. https://doi.org/10.1130/2008.2443(03)

Rodriguez, A.B., Fassell, M.L., Anderson, J.B., 2001. Variations in shoreface progradation and ravinement along the Texas coast, Gulf of Mexico. Sedimentology 48, 837–853. https://doi.org/10.1046/j.1365-3091.2001.00390.x

Rodriguez, A.B., Greene, D.L., Jr., Anderson, J.B., Simms, A.R., 2008b. Response of Mobile Bay and eastern Mississippi Sound, Alabama, to changes in sediment accommodation and accumulation, in: Anderson, J.B., Rodriguez, A.B. (Eds.), Response of Upper Gulf Coast Estuaries to Holocene Climate Change and Sea level Rise. Geological Society of America, p. 0. https://doi.org/10.1130/2008.2443(02)

Shawler, J.L., Ciarletta, D.J., Connell, J.E., Boggs, B.Q., Lorenzo-Trueba, J., Hein, C.J., 2021. Relative influence of antecedent topography and sea level rise on barrier-island migration. Sedimentology 68, 639–669. https://doi.org/10.1111/sed.12798

1033 Simms, A.R., Anderson, J.B., Rodriguez, A.B., Taviani, M., 2008. Mechanisms controlling
1034 environmental change within an estuary: Corpus Christi Bay, Texas, USA, in: Anderson, J.B.,
1035 Rodriguez, A.B. (Eds.), Response of Upper Gulf Coast Estuaries to Holocene Climate Change
1036 and Sea level Rise. Geological Society of America, p. 0.
1037 https://doi.org/10.1130/2008.2443(08)
1038 Simms, A.R., Aryal, N., Miller, L., Yokoyama, Y., 2010. The incised valley of Baffin Bay, Texas: a tale
1039 of two climates. Sedimentology 57, 642–669. https://doi.org/10.1111/j.1365-
1040 3091.2009.01111.x
1041 Siringan, F.P., 1993. Coastal lithosome evolution and preservation during an overall rising sea
1042 level: East Texas gulf coast and continental shelf (Thesis).
1043 Siringan, F.P., Anderson, J.B., 1994. Modern shoreface and inner-shelf storm deposits off the
1044 East Texas Coast, Gulf of Mexico. Journal of Sedimentary Research B64, 99–110.
1045 Siringan, F.P., Anderson, J.B., 1993. Seismic facies, architecture, and evolution of the Bolivar
1046 Roads tidal inlet/delta complex, East Texas Gulf Coast. Journal of Sedimentary Research 63,
1047 794–808. https://doi.org/10.1306/D4267C08-2B26-11D7-8648000102C1865D
1048 Swartz, J., Standring, P., Goff, J.A., Gulick, S., Lowery, C.M., 2022. Coastal River Response to
1049 Transgression: A New Look at the Trinity Incised Valley Using Multi-Resolution Seismic
1050 Imaging.
1051 Swartz, J.M., 2019. Channel processes and products in subaerial and submarine environments
1052 across the Gulf of Mexico. University of Texas, Austin, Tex.
1053 Thomas, M.A., Anderson, J.B., 1994. Sea level Controls on the Facies Architecture of the
1054 Trinity/Sabine Incised-Valley System, Texas Continental Shelf.
1055 Törnqvist, T.E., Bick, S.J., González, J.L., Borg, K. van der, Jong, A.F.M. de, 2004. Tracking the sea
1056 level signature of the 8.2 ka cooling event: New constraints from the Mississippi Delta.
1057 Geophysical Research Letters 31. https://doi.org/10.1029/2004GL021429
1058 Toomey, R.S., Blum, M.D., Valastro, S., 1993. Late Quaternary climates and environments of the
1059 Edwards Plateau, Texas. Global and Planetary Change 7, 299–320.
1060 https://doi.org/10.1016/0921-8181(93)90003-7

1061 Troiani, B.T., Simms, A.R., Dellapenna, T., Piper, E., Yokoyama, Y., 2011. The importance of sea
1062 level and climate change, including changing wind energy, on the evolution of a coastal
1063 estuary: Copano Bay, Texas. Marine Geology 280, 1–19.
1064 Ullman, D.J., Carlson, A.E., Hostetler, S.W., Clark, P.U., Cuzzone, J., Milne, G.A., Winsor, K., Caffee,
1065 M., 2016. Final Laurentide ice-sheet deglaciation and Holocene climate-sea level change.
1066 Quaternary Science Reviews 152, 49–59. https://doi.org/10.1016/j.quascirev.2016.09.014
1067 Vitousek, S., Barnard, P.L., Fletcher, C.H., Frazer, N., Erikson, L., Storlazzi, C.D., 2017. Doubling of
1068 coastal flooding frequency within decades due to sea level rise. Sci Rep 7, 1399.
1069 https://doi.org/10.1038/s41598-017-01362-7
1070 Wagner, A.J., Guilderson, T.P., Slowey, N.C., Cole, J.E., 2009. Pre-Bomb Surface Water
1071 Radiocarbon of the Gulf of Mexico and Caribbean as Recorded in Hermatypic Corals.
1072 Radiocarbon 51, 947–954. https://doi.org/10.1017/S0033822200034020
1073 Wantland, K.F., 1969. Distribution of Modern Brackish-Water Foraminifera in Trinity Bay 93–117.
1074 Weight, R.W.R., Anderson, J.B., Fernandez, R., 2011. Rapid Mud Accumulation On the Central
1075 Texas Shelf Linked To Climate Change and Sea level Rise. Journal of Sedimentary Research 81,
1076 743–764. https://doi.org/10.2110/jsr.2011.57
1077 Wellner, J.S., Sarzalejo, S., Lagoe, M., Anderson, J.B., 2004. Late Quaternary Stratigraphic
1078 Evolution of the West Louisiana/East Texas Continental Shelf, in: Anderson, J.B., Fillon, R.H.
1079 (Eds.), Late Quaternary Stratigraphic Evolution of the Northern Gulf of Mexico Margin. SEPM
1080 Society for Sedimentary Geology, p. 0. https://doi.org/10.2110/pec.04.79.0217
1081 White, W.A., Morton, R.A., Holmes, C.W., 2002. A comparison of factors controlling
1082 sedimentation rates and wetland loss in fluvial–deltaic systems, Texas Gulf coast.
1083 Geomorphology 44, 47–66. https://doi.org/10.1016/S0169-555X(01)00140-4
1084 Williams, H.F.L., 1994. Intertidal Benthic Foraminiferal Biofacies on the Central Gulf Coast of
1085 Texas: Modern Distribution and Application to Sea Level Reconstruction. Micropaleontology
1086 40, 169–183. https://doi.org/10.2307/1485774
1087 Woo, H.J., Culver, S.J., Oertel, G.F., 1997. Benthic Foraminiferal Communities of a Barrier-Lagoon
1088 System, Virginia, U.S.A. Journal of Coastal Research 13, 1192–1200.
1089

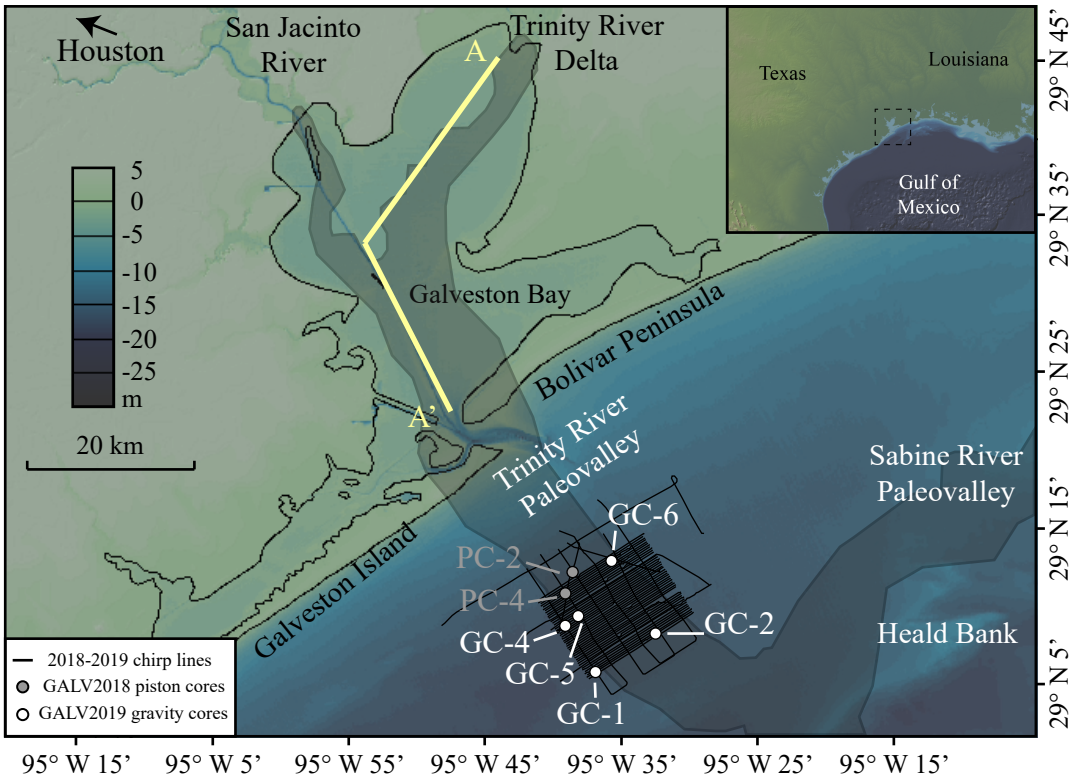


Figure 1. Study area offshore Galveston Bay, Texas, with Trinity River incised valley (gray outline), A-A' profile of cross-section shown in Figure 4 from Anderson et al. (2008), high-resolution seismic lines (black lines), 2018 piston cores (gray circles), and 2019 gravity cores (white circles). Base map made with GeoMapApp (www.geomapapp.org) and the National Centers for Environmental Information (formerly NGDC) Coastal Relief Model (Divens and Metzger, 2001).

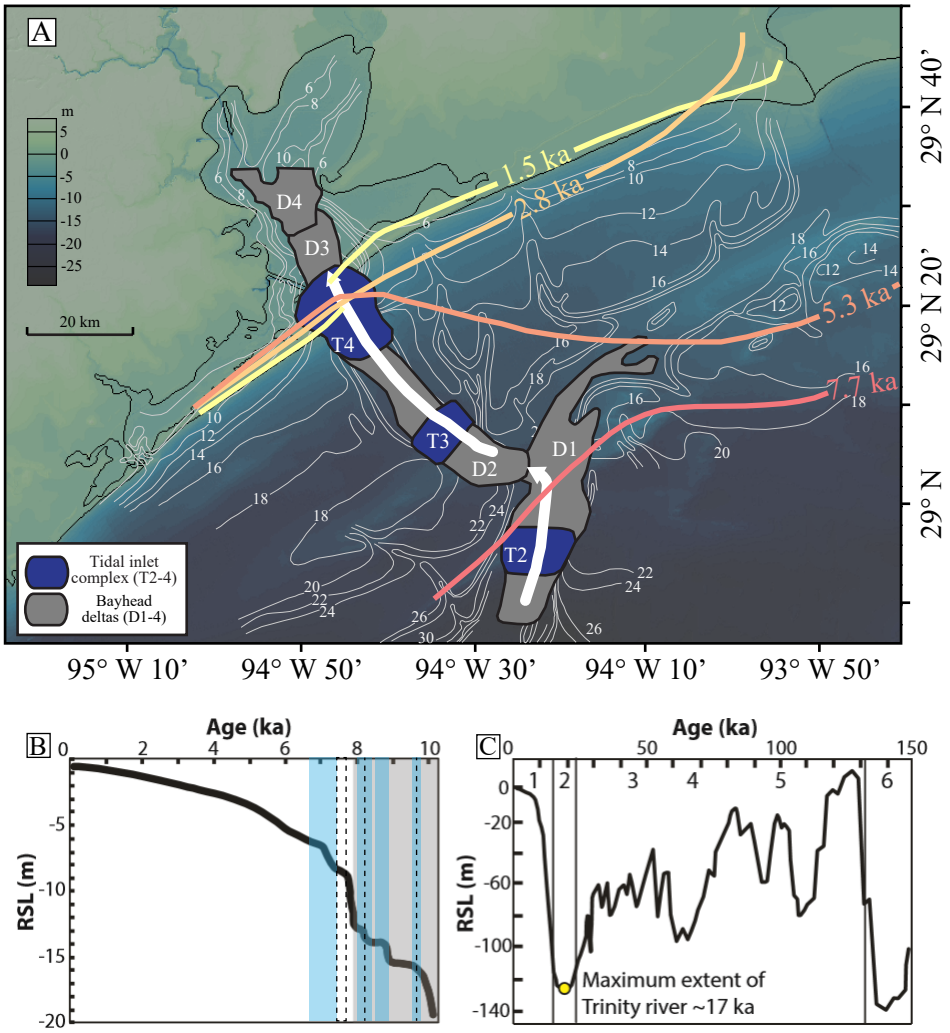


Figure 2. A) Map of modern Galveston Bay with topographic contours of the Holocene-Pleistocene surface (redrawn from Siringan, 1993), backstepping bayhead deltas with associated tidal inlets infilling the Trinity River incised valley during Holocene trangsgression (modified from Swartz, 2019), and the current paleoshoreline model for Galveston Bay (redrawn from Rodriguez et al., 2004). Base map made with GeoMapApp (www.geomapapp.org) and the National Centers for Environmental Information (formerly NGDC) Coastal Relief Model (Divens and Metzger, 2001). B) Sea level rise over the last 10 kyr with periods of rapid sea level rise identified by Milliken et al. (2008a) (shaded blue) and rapid sea level rise in Galveston Bay, Texas, identified by Anderson et al. (2008) (dashed lines). C) Holocene sea level curve over last 150 kyr showing Marine Isotope Stages 1-6 and maximum lowstand for the Trinity River occurring approximately 17 ka (modified from Swartz, 2019).

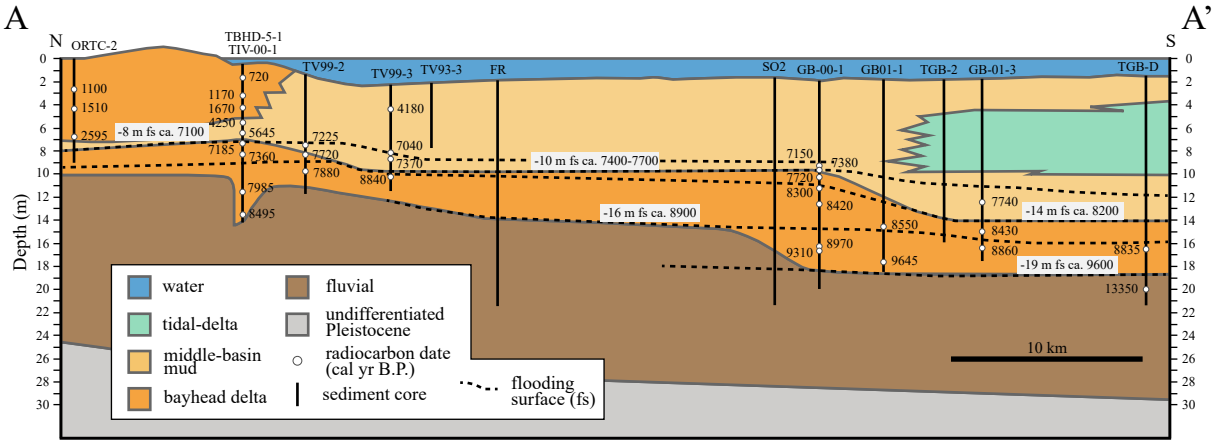


Figure 3. Cross section of the Trinity River Paleovalley in modern Galveston Bay, Texas (location in Figure 1), compiled from seismic and core data analyzed by Anderson Group displaying prominent sedimentary facies and flooding surfaces with radiocrabon ages (redrawn from Anderson et al., 2008).

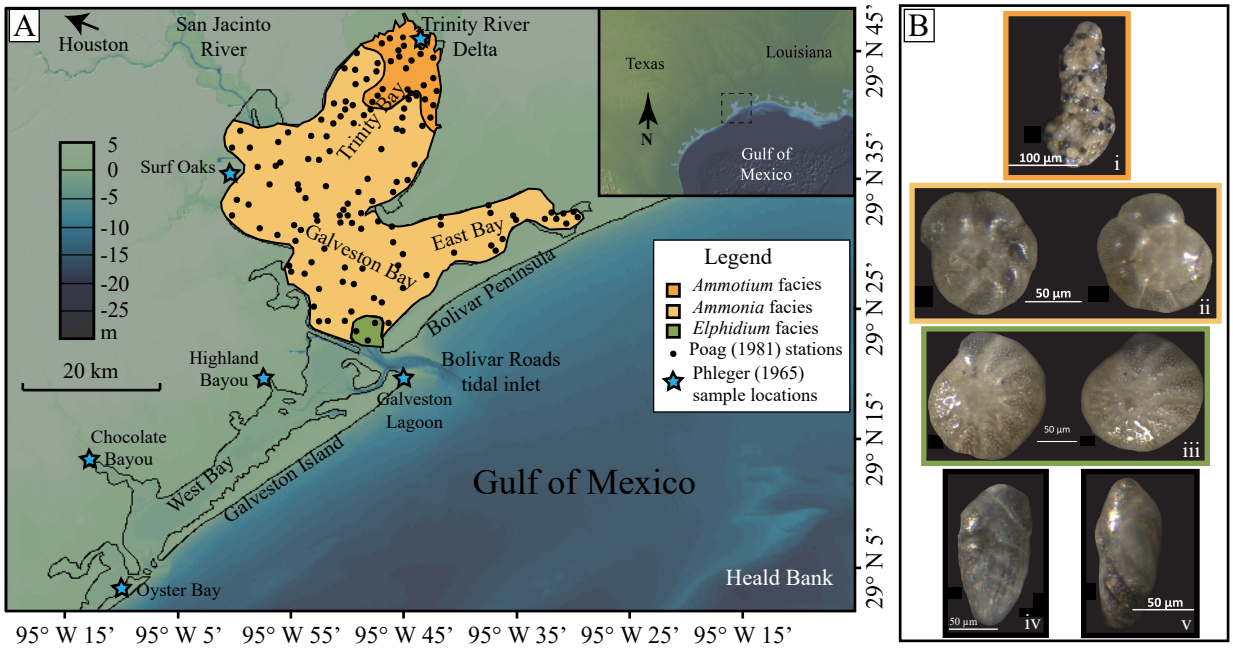


Figure 4. Foraminiferal predominance facies of Galveston Bay, Texas, based on Poag (1981). A) Map of Galveston Bay, Texas, showing areas within the modern estuary that are dominated by specific genera of foraminifera, and locations of marshes (blue stars) studied by Phleger (1965). B) Images of dominant genera of foraminifera: i) *Ammotium salsum* (orange; upper bay facies), ii) *Ammonia* sp. (yellow-orange; central bay facies), iii) *Elphidium* sp. (green; outer bay facies), iv and v) *Bolivina* sp. and *Bulimina* sp., respectively, which are diagnostic genera for inner shelf facies (Culver, 1988) (modified from Poag, 1981, and Phleger, 1965). Figure made with GeoMapApp (www.geomapapp.org) and the National Centers for Environmental Information (formerly NGDC) Coastal Relief Model (Divens and Metzger, 2001).

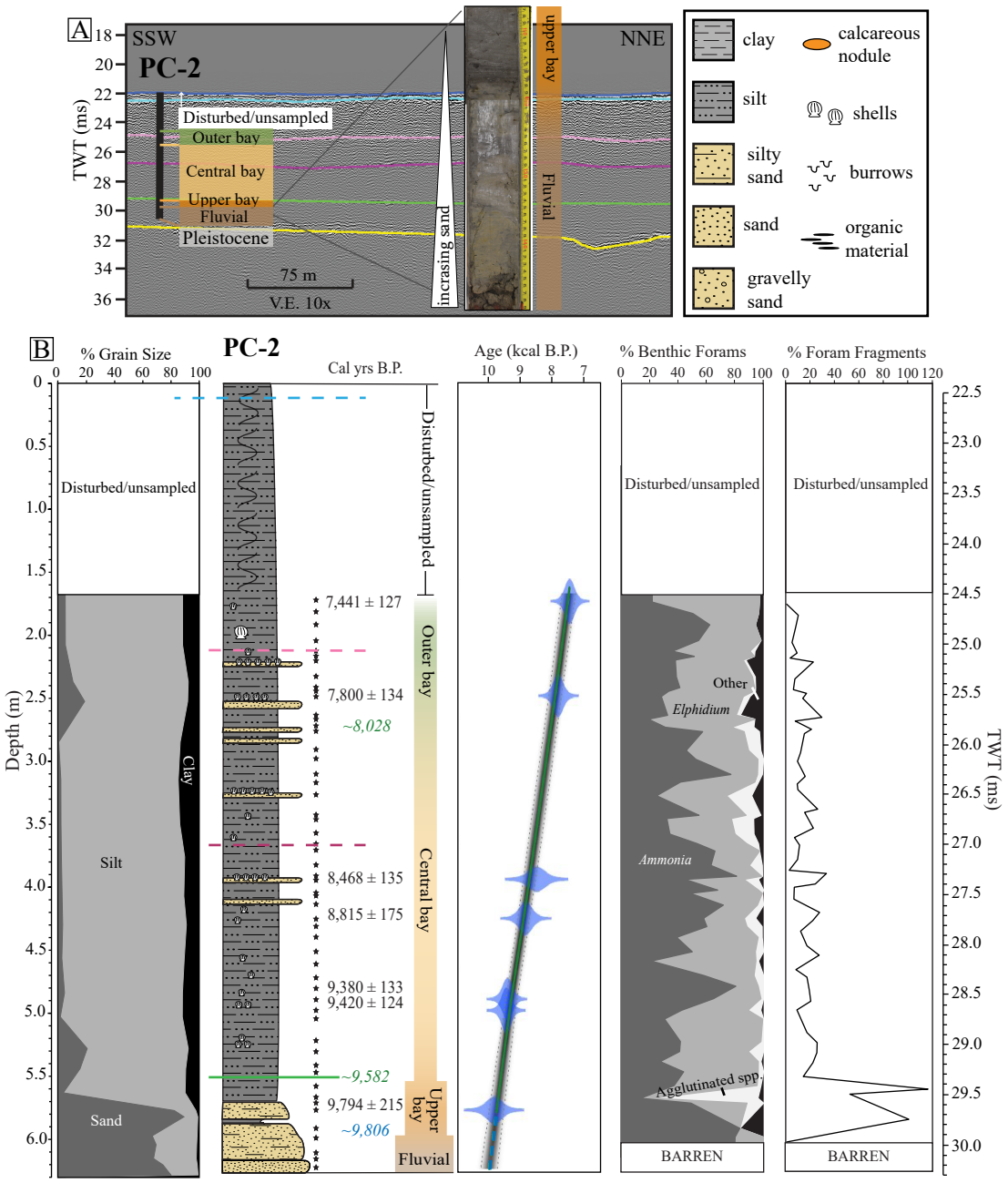


Figure 5. Piston Core 2 (PC-2). A) Interpreted seismic data with approximate depth of penetration for PC-2 (location in Figure 1). Seismic interpretation from Burstein et al. (2022) (VE = vertical exaggeration) with core image of fluvial to upper bay transition. Seismic interpretation is depicted separately from foraminiferal facies transitions because it does not line up exactly in this core. B) Grain size abundance and stratigraphic column of PC-2 displaying sample locations (black stars), carbon dates (black text), and interpolated (italicized green text) and extrapolated (italicized blue text) ages from age model. Age model based off of radiocarbon ages (blue ovals tapering to error range), with mean age depicted by solid dark green line for interpolated ages, light blue dashed line for extrapolated ages, and gray scale out to 95% confidence interval predicted by the model. Interpreted depositional facies based off of foraminiferal assemblage abundances and percent foram fragments. Two-way travel time scale for stratigraphic column in ms calculated from approximate seismic velocity of 1,525 m/s starting at time of seafloor.

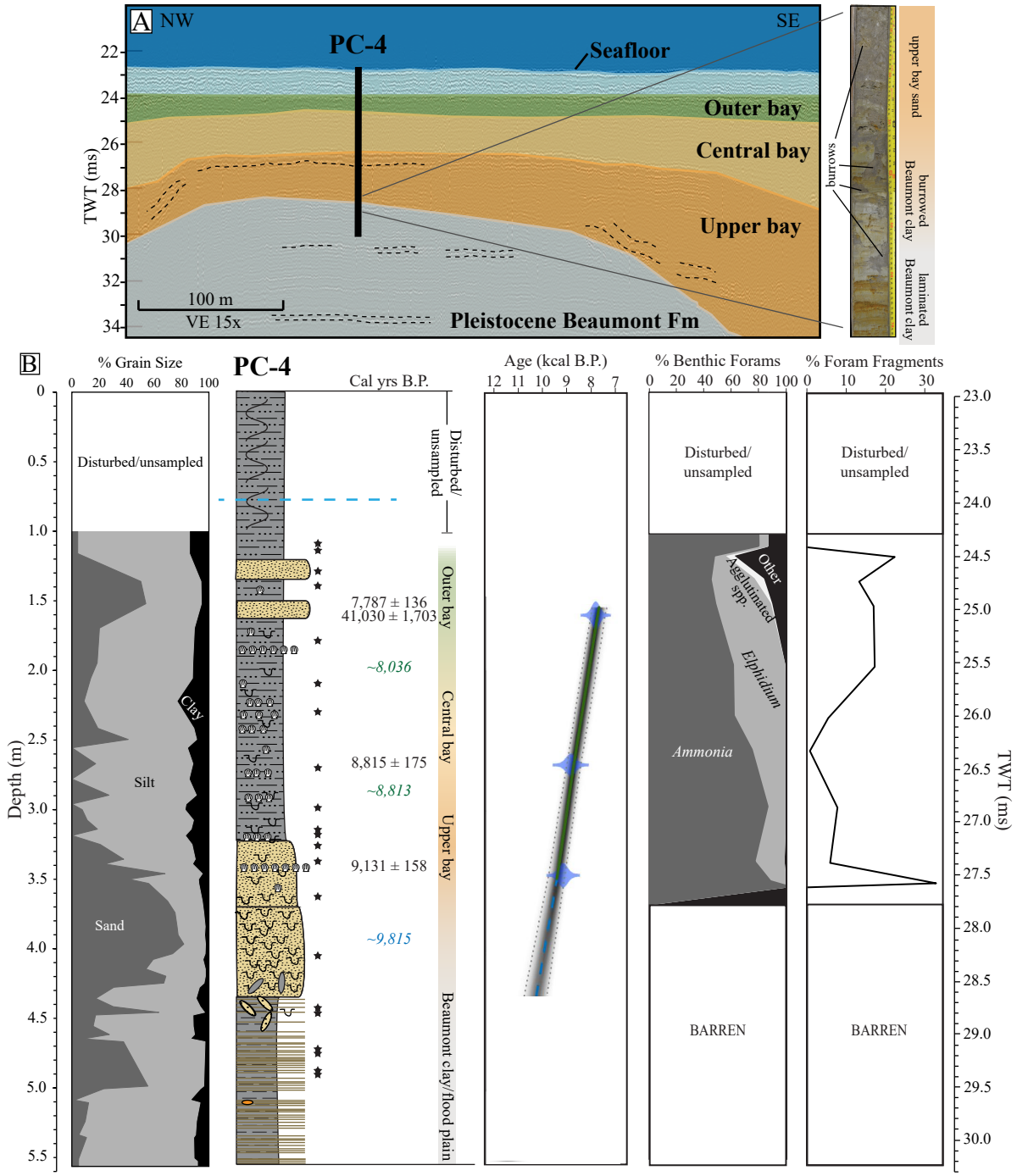


Figure 6. Piston Core 4 (PC-4). A) Interpreted seismic data with approximated depth for PC-4 into a Pleistocene terrace (location in Figure 1) overlain by paleoenvironment based on micropaleontologic data. Seismic interpretation from Burstein et al. (2022) (VE = vertical exaggeration) with core image showing transition from Pleistocene clay to upper bay sediments. B) Grain size abundance and stratigraphic column with sample locations (black stars), carbon dates (black text), and interpolated (italicized green text) and extrapolated (blue text) ages from age model. Age model based off of radiocarbon ages (blue ovals tapering to error range), with mean age depicted by dark green solid line for interpolated ages, light blue dashed line for extrapolated ages, and gray scale out to 95% confidence interval predicted by the model. Interpreted depositional facies based off of foraminiferal assemblage abundances and percent foram fragments. Two-way travel time scale for stratigraphic column in ms calculated from approximate seismic velocity of 1,525 m/s starting at time of seafloor.

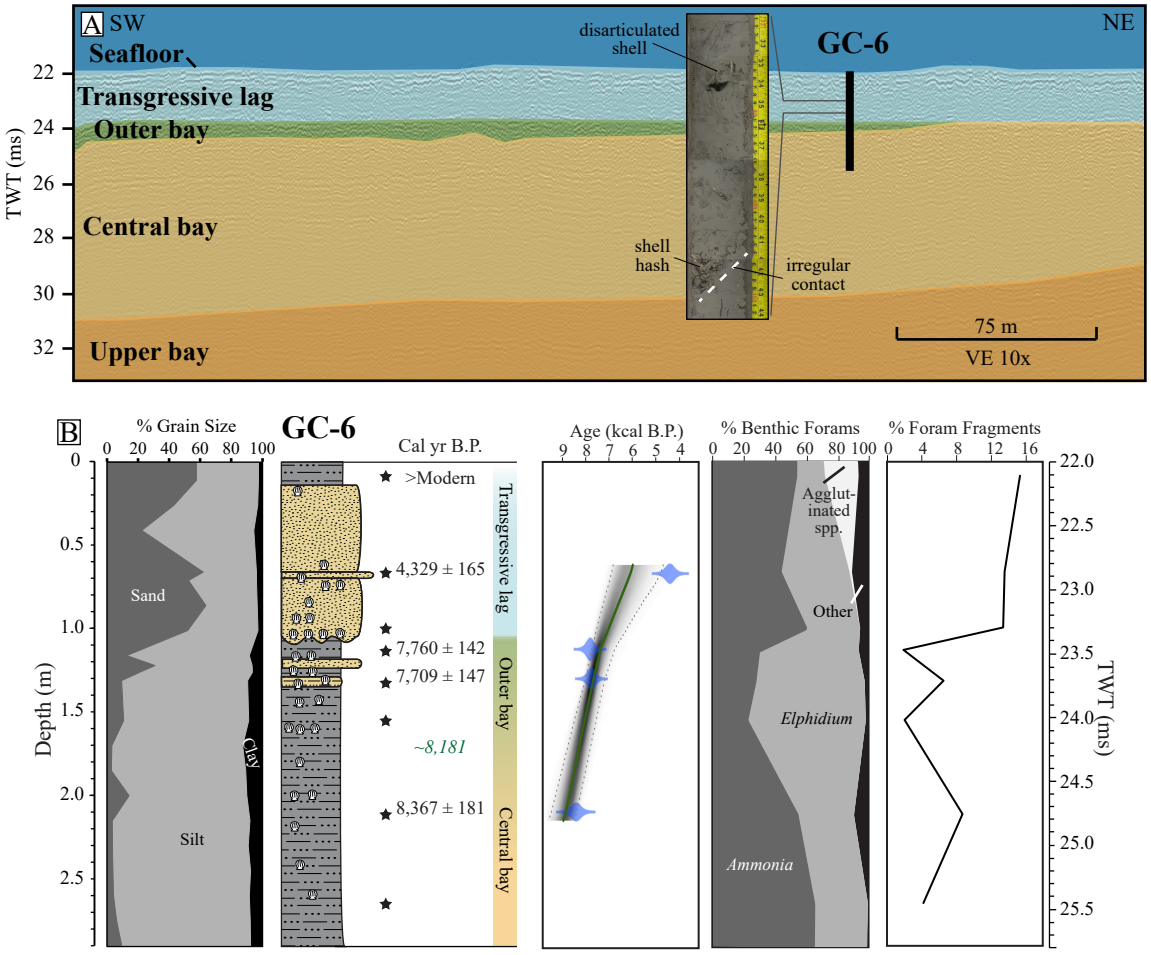


Figure 7. Gravity Core 6 (GC-6). A) Interpreted seismic data with approximate depth of penetration for GC-6 (location in Figure 1), overlain by paleoenvironment based on micropaleontologic data, and core image of transgressive lag deposit. Seismic interpretation from Burstein et al. (2022) (VE = vertical exaggeration). B) Grain size abundance and stratigraphic column with sample locations (black stars), radiocarbon dates (black text), and interpolated ages (italicized green text) based off of age model. Age model based off of radiocarbon ages (blue ovals tapering to error range), with mean age depicted by solid green line and gray scale out to 95% confidence interval predicted by the model. Interpreted depositional facies based off of foraminiferal assemblage abundances and percent foram fragments. Two-way travel time scale for stratigraphic column in ms calculated from approximate seismic velocity of 1,525 m/s starting at time of seafloor.

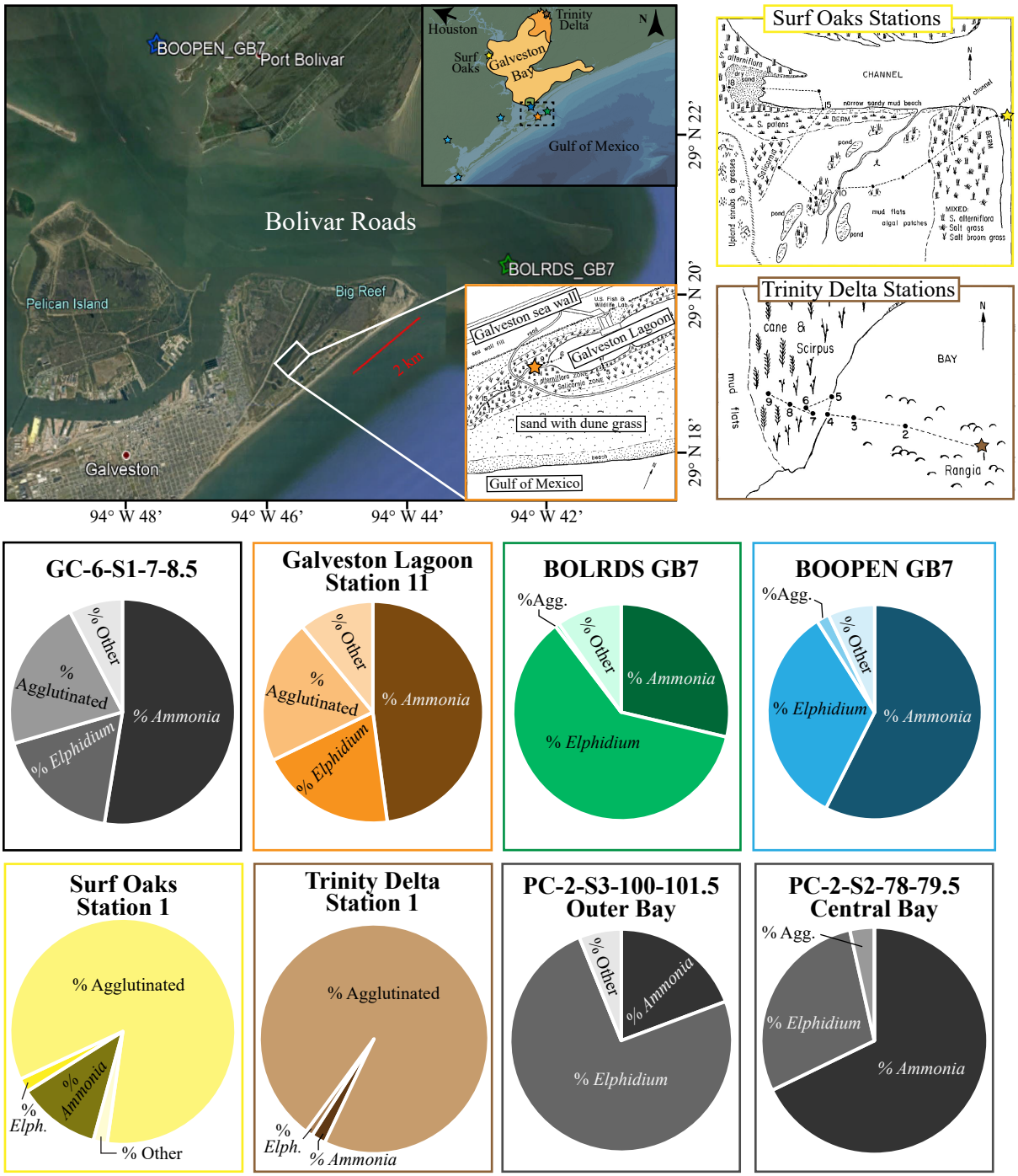


Figure 8. Comparison of GC-6 upper sample (7-8.5 cm) to modern foram assemblages: Galveston Lagoon Station 11 (orange), Surf Oaks Station 1 (yellow), and Trinity Delta Station 1 (brown) analyzed by Phleger (1965); BOLRDS GB7 grab sample taken from the outer edge of the tidal inlet (green); BOOPEN GB7 grab sample taken from the inner edge of the tidal inlet (blue); and two samples from PC-2 representing the outer bay and central bay sediments (grayscale). The Phleger (1965) station samples come from saltmarsh locations surrounding Galveston Bay, with Galveston Lagoon as the most seaward station located on Galveston Island, Surf Oaks on the western edge of the bay, and Trinity Delta as the most landward station. The Station 11 sample is the closest approximation to the GC-6 sample. Basemap image source Google Earth (2021); drawn maps of marsh locations from Phleger (1965).

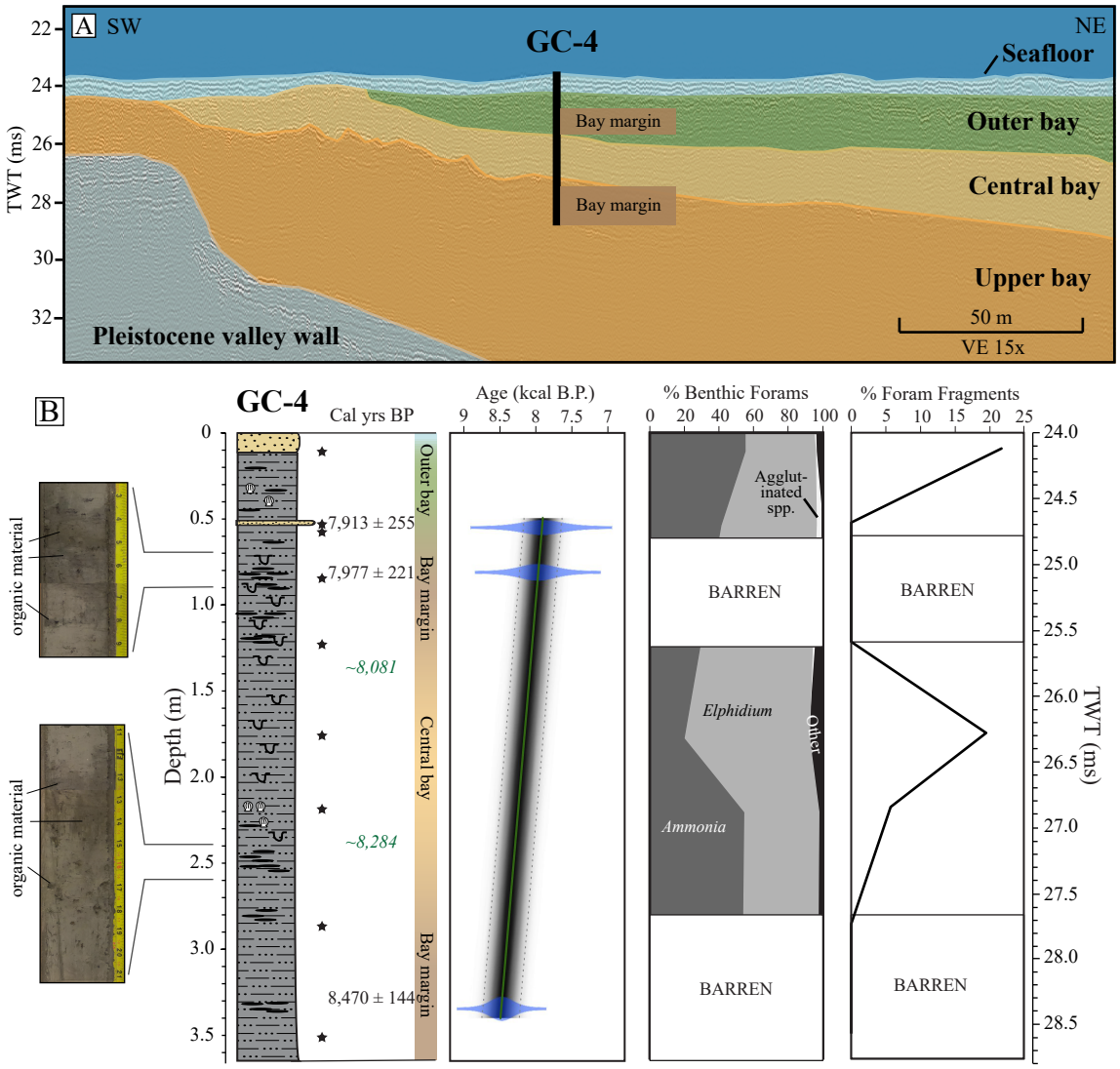


Figure 9. Gravity Core 4. A) Interpreted seismic data with approximate depth of penetration for GC-4 (location in Figure 1), overlain by paleoenvironment based on micropaleontologic data, including intervals interpreted as bay margin based on lack of foraminifera in core sediments. Seismic interpretation from Burstein et al. (2022) (VE = vertical exaggeration). B) Partial core images and full stratigraphic column of GC-4 showing samples (black stars) with radiocarbon ages (black text), interpolated ages (italicized green text) from age model. Age model based off of radiocarbon ages (blue ovals tapering to error range), with mean age depicted by solid green line and gray scale out to 95% confidence interval predicted by the model. Interpreted depositional facies based off of foraminiferal assemblage abundances and percent foram fragments. Two-way travel time scale for stratigraphic column in ms calculated from approximate seismic velocity of 1,525 m/s starting at time of seafloor.

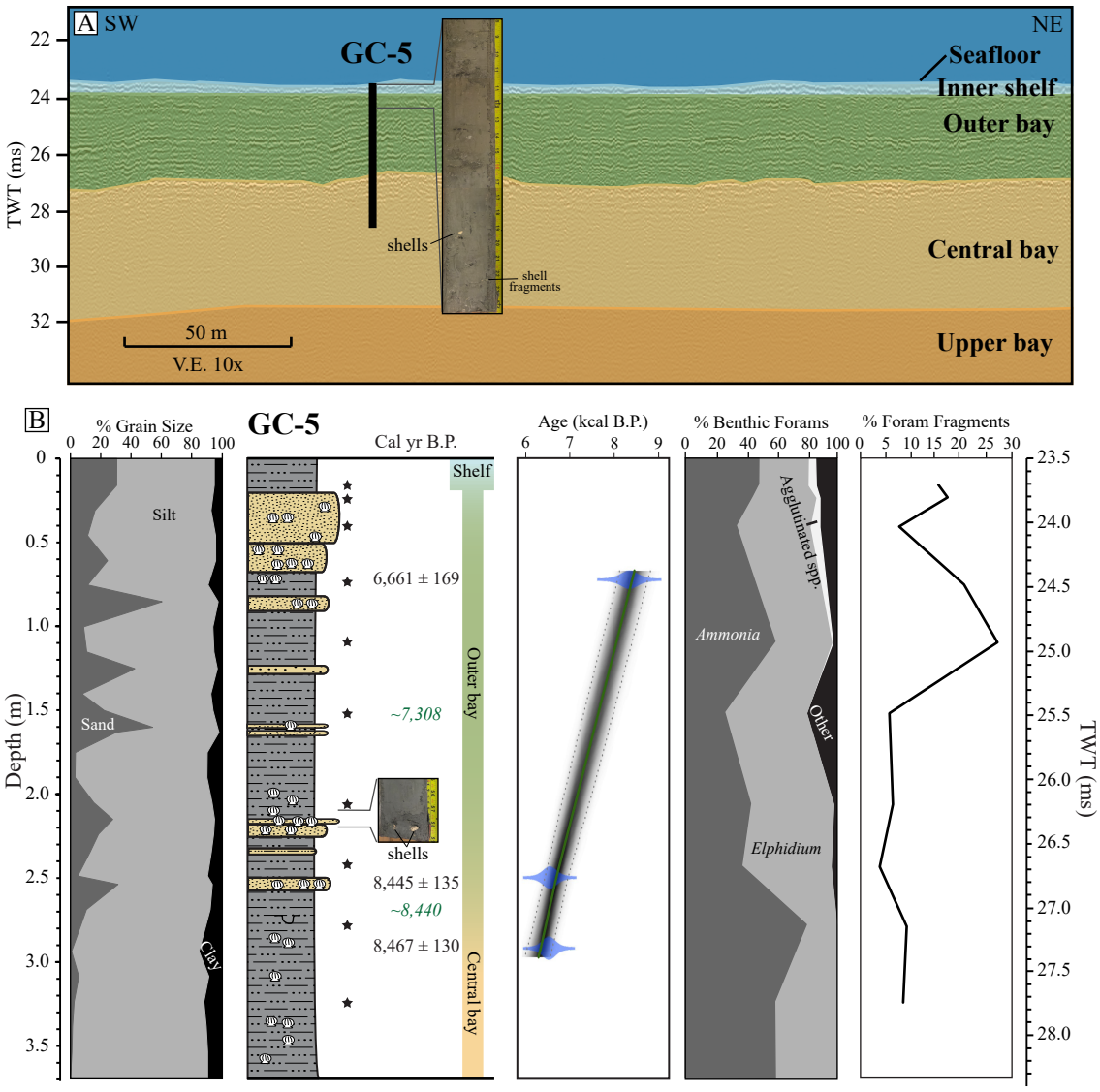


Figure 10. Gravity Core 5 (GC-5). A) Interpreted seismic data with approximate depth of penetration for GC-5 (location in Figure 1), overlain by paleoenvironment based on micropaleontologic data, and core image of sandy outer bay and inner shelf sediments. Seismic interpretation from Burstein et al. (2022) (VE = vertical exaggeration). B) Grain size abundance and and stratigraphic column of GC-5 with core image of sandy sediments and shell fragments and samples (black stars) with radiocarbon ages (black text), and interpolated ages (italicized green text) from age model. Age model based off of radiocarbon ages (blue ovals tapering to error range), with mean age depicted by solid green line and gray scale out to 95% confidence interval predicted by the model. Interpreted depositional facies based off of foraminiferal assemblage abundances and percent foram fragments. Two-way travel time scale for stratigraphic column in ms calculated from approximate seismic velocity of 1,525 m/s starting at time of seafloor.

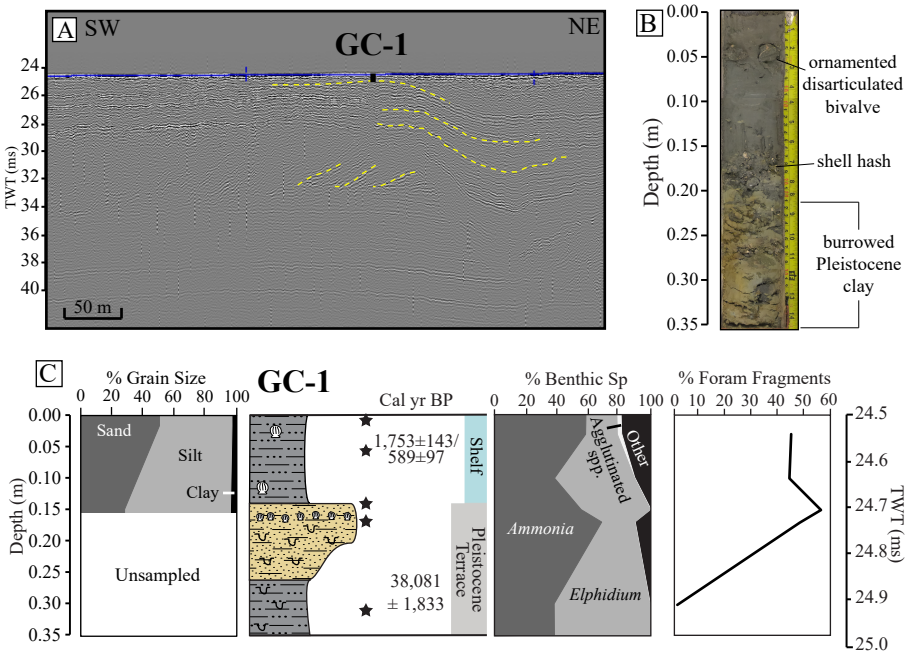


Figure 11. Gravity core 1 (GC-1). A) Uninterpreted seismic line showing location of GC-1 short core where it penetrated a high-elevation Pleistocene terrace. Yellow dashed lines show approximated interpretation of draped sediments and dipping reflectors. B) Image of entire core. C) Grain size abundance (only upper 15 cm of core sampled for grain size) and stratigraphic column of GC-1 showing sample locations (black stars), radiocarbon dates, and interpreted depositional environments based on lithology, and foraminiferal assemblages and fragmentation. Two-way travel time (TWT) scale calculated based on approximate seismic velocity of 1,525 m/s starting at time of seafloor.

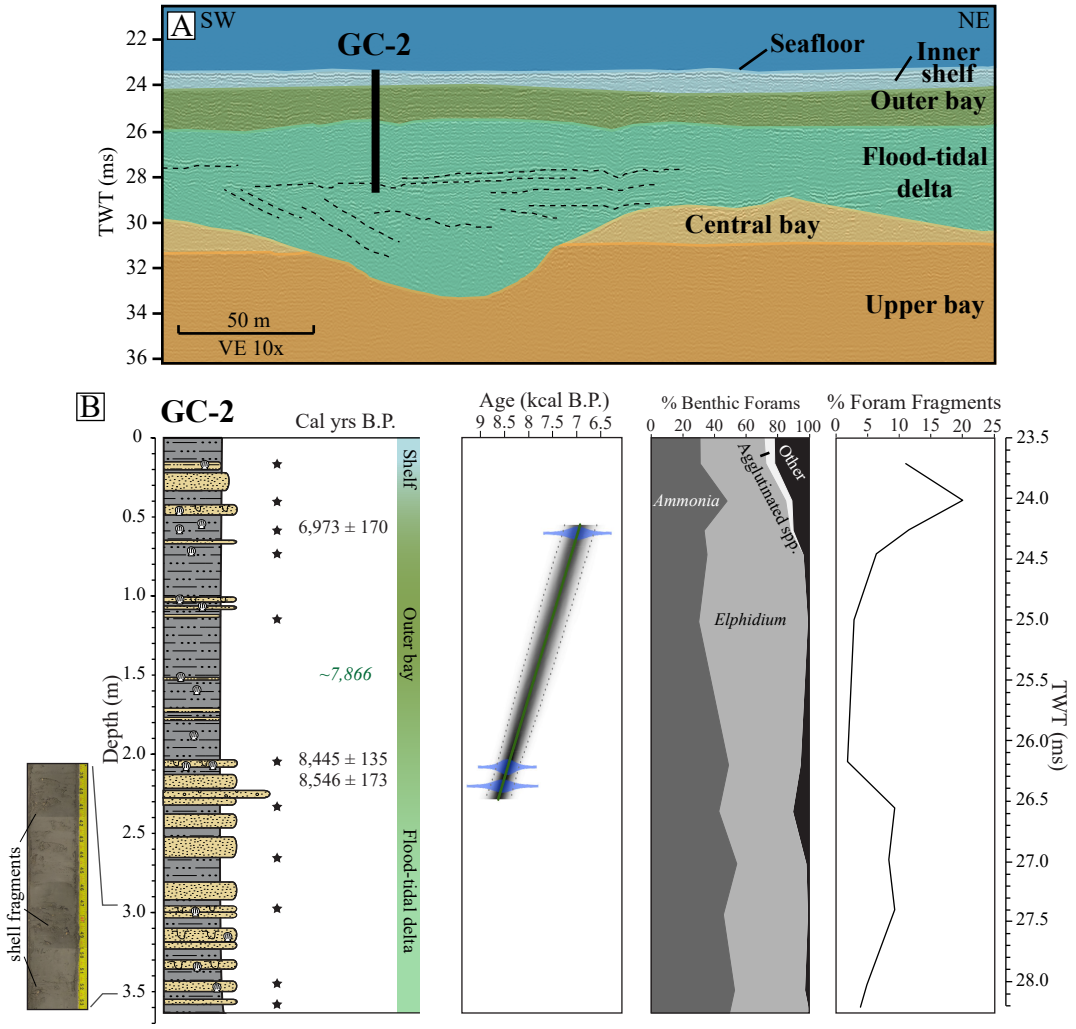
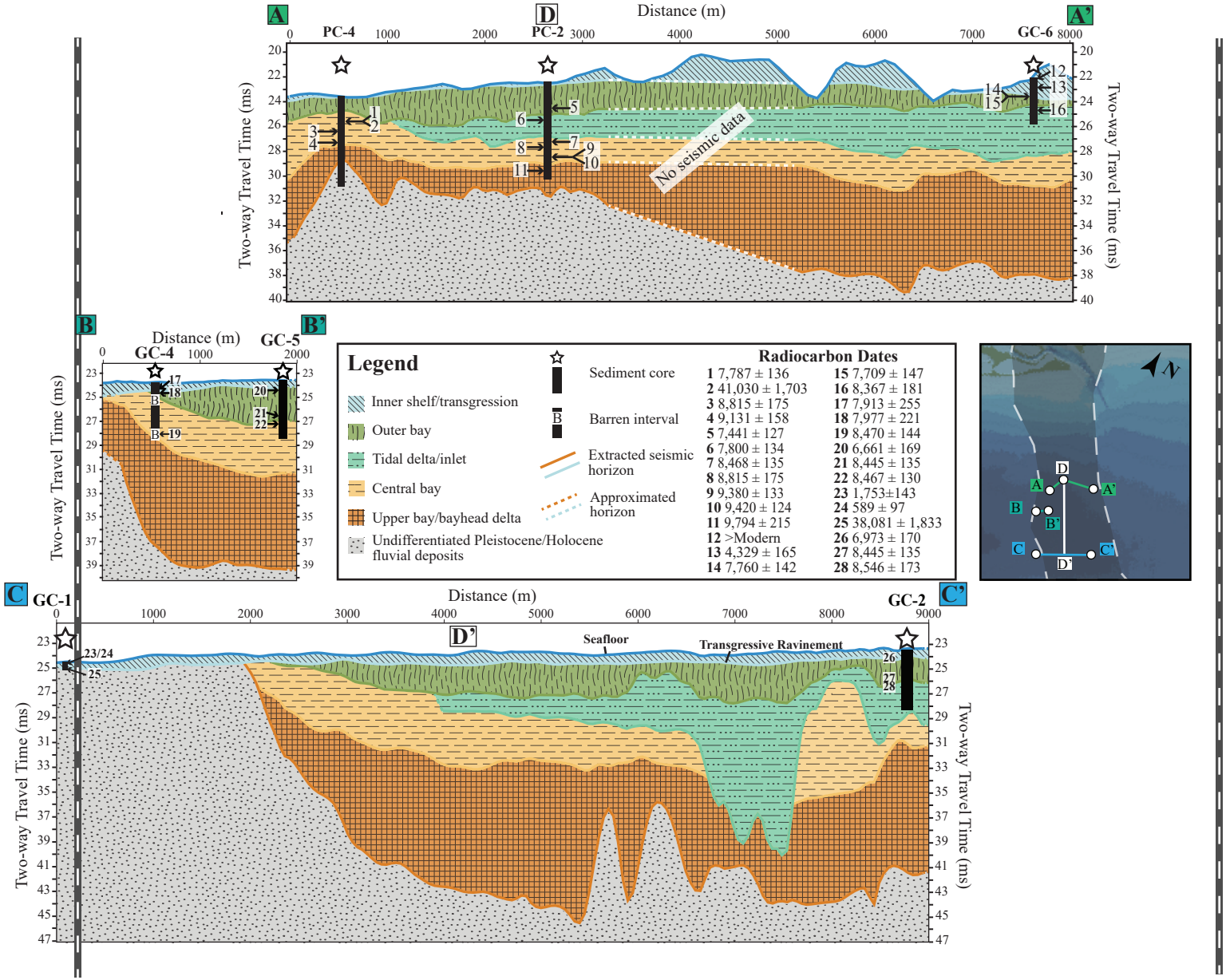


Figure 12. Gravity core 2 (GC-2). A) Interpreted seismic data with approximate depth of penetration for GC-2 (location in Figure 1), overlain by paleoenvironment based on micropaleontologic data. Seismic interpretation from Burstein et al. (2022) (VE = vertical exaggeration). B) Partial core image and full stratigraphic column with sample locations (black stars), radiocarbon dates (black text), interpolated ages (italicized green text) from age model. Age model based off of radiocarbon ages (blue ovals tapering to error range), with mean age depicted by solid green line and gray scale out to 95% confidence interval predicted by the model. Interpreted depositional facies based off of foraminiferal assemblage abundances and percent foram fragments. Two-way travel time scale for stratigraphic column in ms calculated from approximate seismic velocity of 1,525 m/s starting at time of


A
A'
D
Distance (m)
PC-4
PC-2
GC-6
Two-way Travel Time (ms)
No seismic data
B
B'
GC-4
GC-5
C
C'
GC-1
GC-2
D'
Seafloor
Transgressive Ravinement
Legend
Inner shelf/transgression
Outer bay
Tidal delta/inlet
Central bay
Upper bay/bayhead delta
Undifferentiated Pleistocene/Holocene fluvial deposits
Sediment core
Barren interval
Extracted seismic horizon
Approximated horizon
Radiocarbon Dates
1 7,787 ± 136
2 41,030 ± 1,703
3 8,815 ± 175
4 9,131 ± 158
5 7,441 ± 127
6 7,800 ± 134
7 8,468 ± 135
8 8,815 ± 175
9 9,380 ± 133
10 9,420 ± 124
11 9,794 ± 215
12 >Modern
13 4,329 ± 165
14 7,760 ± 142
15 7,709 ± 147
16 8,367 ± 181
17 7,913 ± 255
18 7,977 ± 221
19 8,470 ± 144
20 6,661 ± 169
21 8,445 ± 135
22 8,467 ± 130
23 1,753±143
24 589 ± 97
25 38,081 ± 1,833
26 6,973 ± 170
27 8,445 ± 135
28 8,546 ± 173
N

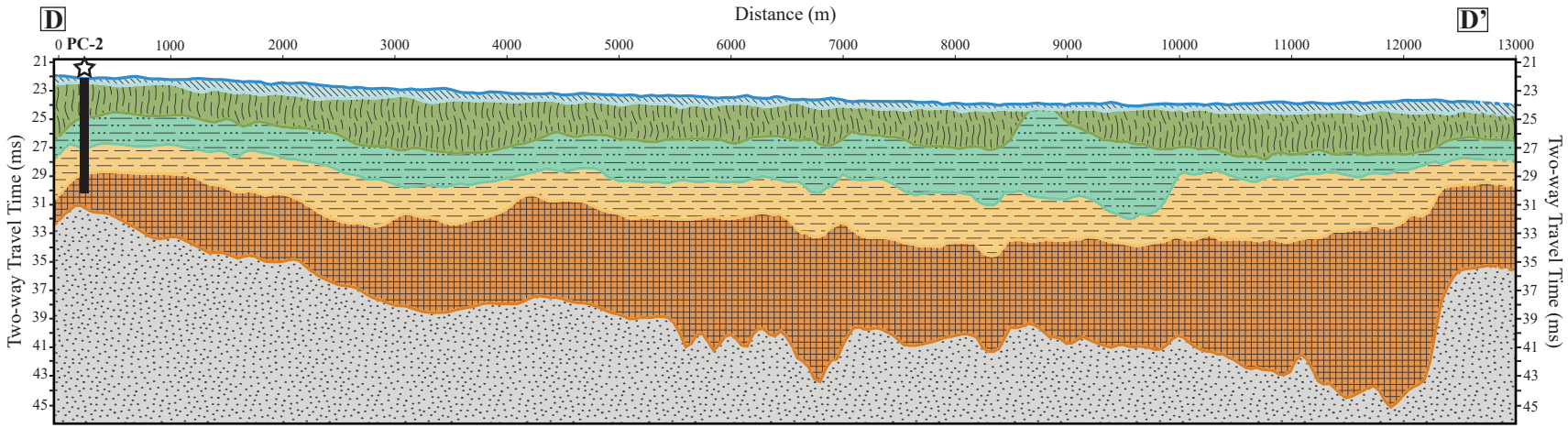


Figure 13. Fence diagram showing depositional environment between cores cores within our study area. Depositional facies across the Trinity River Paleovalley are approximated from extracted seismic horizons in Burstein et al. (2022). Horizons were interpolated for a portion of profile A-A' between PC-2 and GC-6 where there is no seismic data available. Core depths approximate from two-way travel time conversion using approximated velocity of 1,525 m/s. Basemap for core and profile locations obtained from Global Multi-Resolution Topography Data Synthesis (Ryan et al., 2009) via GeoMapApp (www.geomapapp.org).

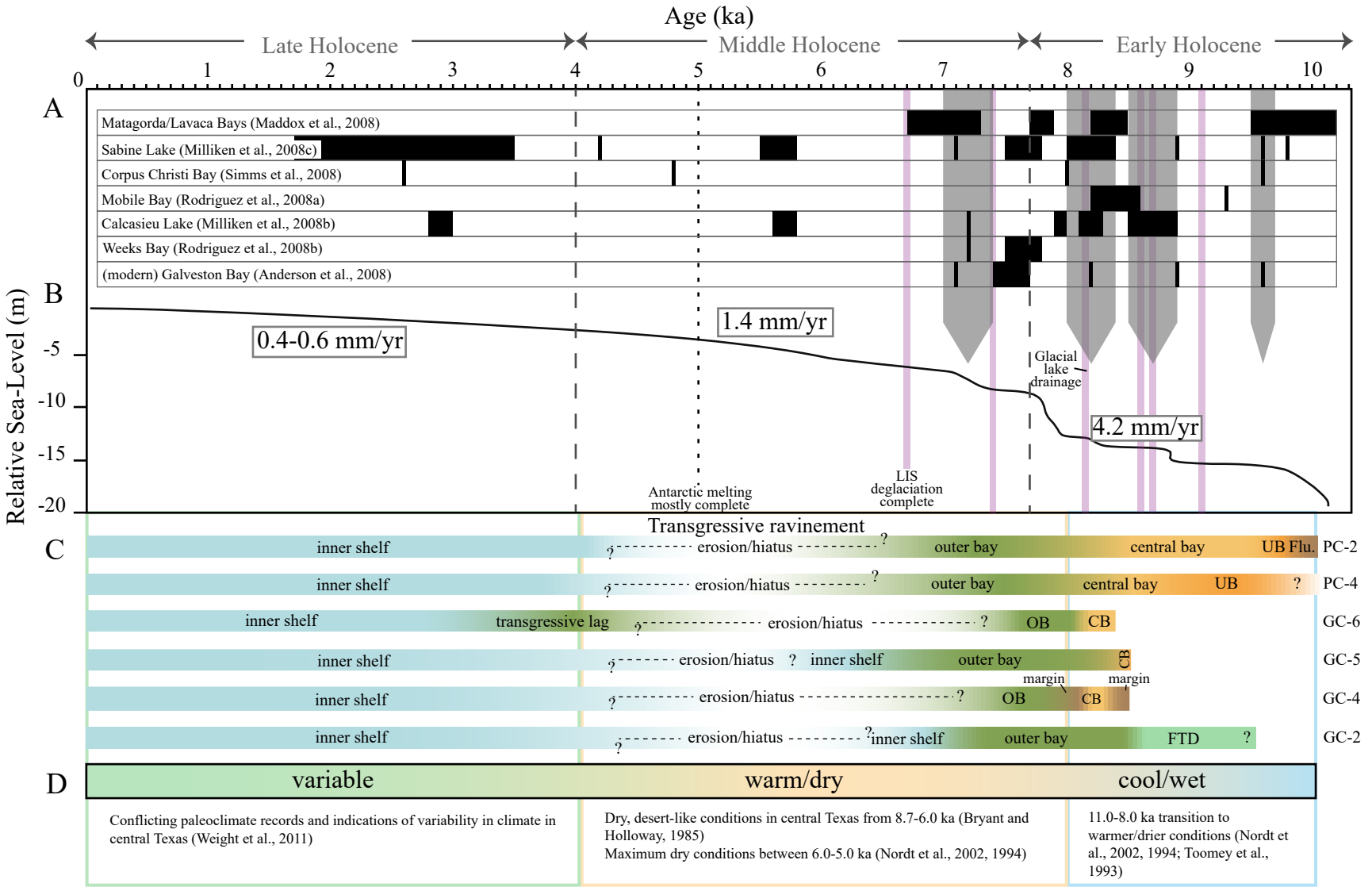


Figure 14. Timeline of environmental change and sea-level rise in Galveston paleostuary. A) Flooding events from other Gulf Coast Bays. B) Gulf Coast Holocene sea level curve (modified from Milliken et al., 2008a) containing prominent North American glacial events (purple) identified in Jennings et al. (2015), northern Gulf of Mexico flooding events (gray) from Milliken et al. (2008a), and rates of sea-level rise for the early, middle, and late Holocene (boxed in grey) from Anderson et al. (2022). C) Compilation of environmental change within Trinity River paleovalley cores for our study area and approximated period of transgressive erosion. D) Gulf Coast dominant climate regimes for the Holocene (modified from Weight et al., 2011). A majority of environmental transitions take place during a cool/wet climate when sea-level rise was more rapid, while significant transgressive erosion took place during a warm/dry period when sea-level rise slowed.

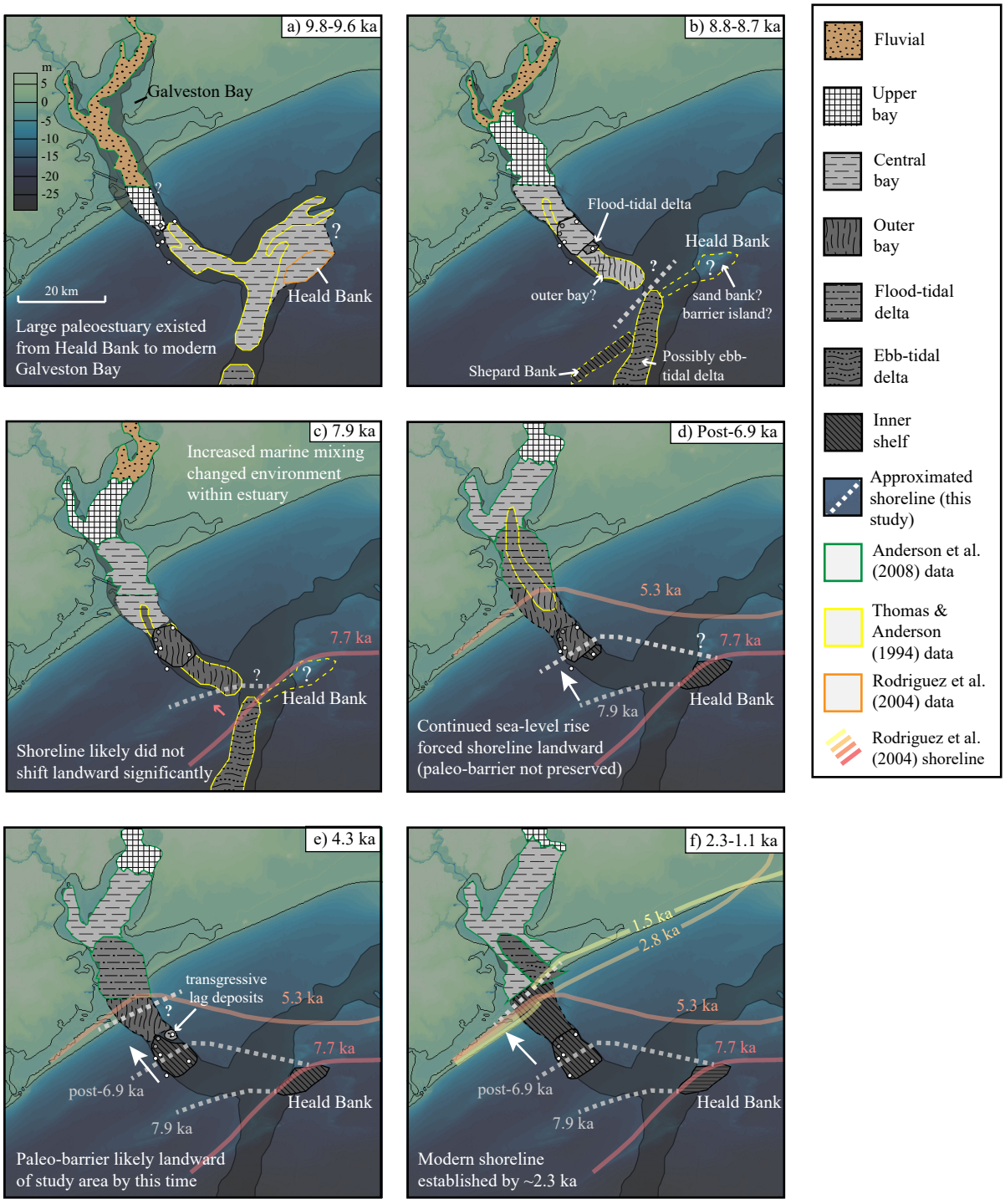


Figure 15. Summary of paleoenvironmental change of Holocene estuary offshore Galveston Bay, Texas. Environmental facies at specific periods of time are based on micropaleontological analysis of cores in study areas and combined with previous research (outlined in green, yellow, and orange), and inferences were made between these study areas (dashed outlines). Facies are mapped within the bounds of the incised valley, but likely extended beyond those boundaries; however, the outer boundaries are difficult to determine due to probable removal of sediments during marine transgression. Paleoshorelines are estimated based on proximity to tidal delta and outer bay environments, and identification of probable washover sediments in cores.